iScience

CellPress
OPEN ACCESS

Article

Body Mass Dynamics Is Determined by the Metabolic Ohm's Law and Adipocyte-Autonomous Fat Mass Homeostasis

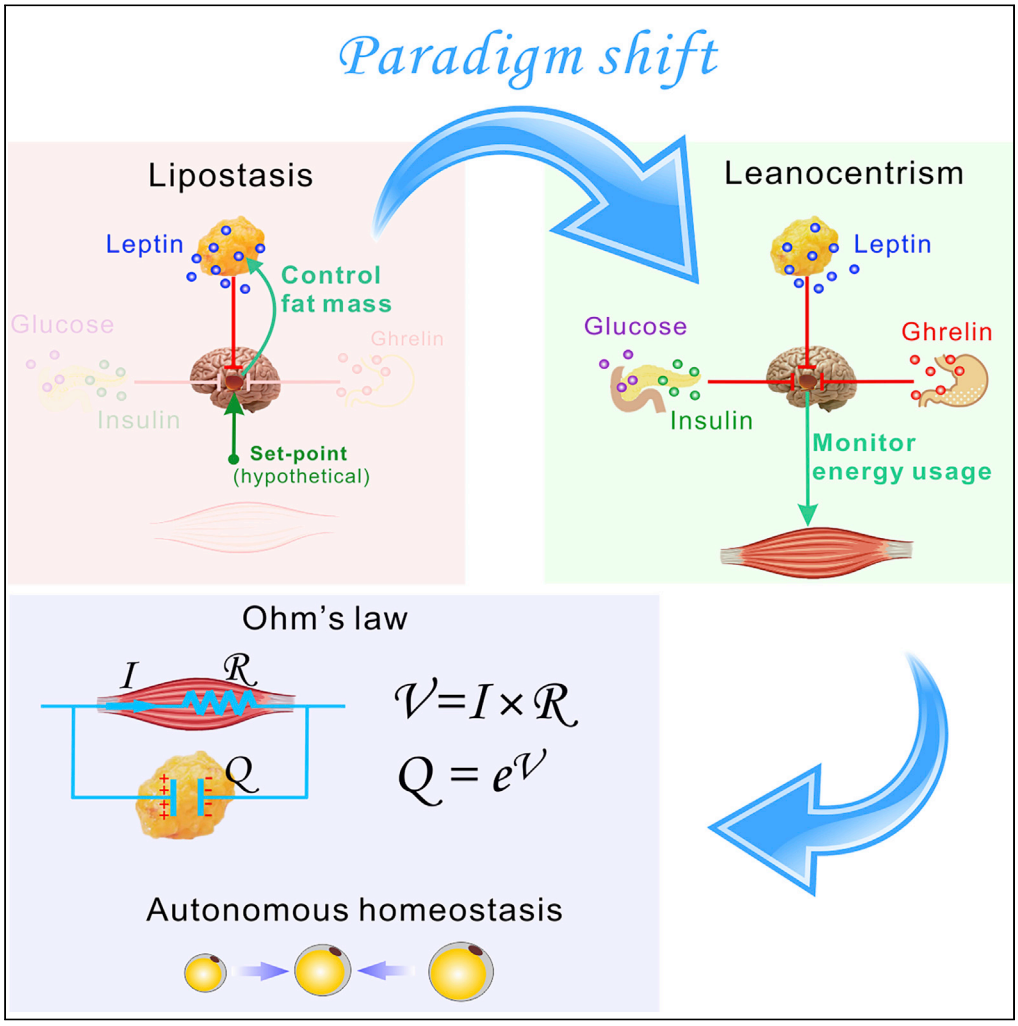

Guanyu Wang

wanggy@sustech.edu.cn

HIGHLIGHTS

Paradigm shift from lipostatic set-point to leanocentric locking-point

Fat mass homeostasis is a cell-autonomous property of adipocytes

Fat mass change is governed by metabolic Ohm's law

Peripheral insulin resistance is crucial for long-term body protection

Wang, iScience *23*, 101176
June 26, 2020
https://doi.org/10.1016/j.isci.2020.101176

iScience

CellPress
OPEN ACCESS

Article

Body Mass Dynamics Is Determined by the Metabolic Ohm's Law and Adipocyte-Autonomous Fat Mass Homeostasis

Guanyu Wang[1,2,3,4,5,*]

SUMMARY

An ODE model integrating metabolic mechanisms with clinical data reveals an Ohm's law governing lifetime body mass dynamics, where fat and lean tissues are analogous to a parallel nonlinear capacitor and resistor, respectively. The law unexpectedly decouples weight stability (a cell-autonomous property of adipocytes) and weight change (a parabolic trajectory governed by Ohm's law). In middle age, insulin resistance causes fat accumulation to avoid excessive body shrinkage in old age. Moderate middle-age spread is thus natural, not an anomaly caused by hypothalamic defects, as proposed by lipostatic theory. These discoveries provide valuable insights into health care practices such as weight control and health assessment, explain certain observed phenomena, make testable predictions, and may help to resolve major conundrums in the field. The ODE model, which is more comprehensive than Ohm's law, is useful to study metabolism at the detailed microscopic levels.

INTRODUCTION

Our knowledge of metabolism is highly detailed, with fine mechanisms delineated at all biological levels and with large amounts of data being generated every day. However, even commonplace phenomena are still difficult to explain. Why does a middle-aged person gain weight much more easily than a younger person? What drives "middle-age spread?" Why is middle-age spread often followed by "old-age shrinkage?" Does the obvious change in weight defy the concept of weight stability? If not, what underlies weight stability? The existing answers to such questions are largely unclear or wrong, not because the molecular details are insufficient but because of the lack of physical laws that abstract away non-essentials. Such a law could be very powerful (West et al., 1997, 2002; Scott and Hwa, 2011).

We aimed to establish a law governing body weight dynamics. Note that the change in body weight is primarily due to the change in fat mass (FM) because the change in lean mass (LM) is much smaller, and weight stability is essentially related to fat mass homeostasis. To avoid proposing too simplistic a law, we studied metabolism at multiple biological levels from molecules to the organism (Wang, 2010, 2012, 2014; Li and Wang, 2014). In this paper, an ordinary differential equation (ODE) model was first developed to integrate the complexities. By using the model to analyze clinical data, we distilled a metabolic Ohm's law, which enables clear and quantifiable answers to the above questions. In particular, it reveals the parabolic trajectory of the weight change of an average sedentary adult (Figure 1E).

Despite the clear pattern of weight change over the lifespan, on a shorter (but still long) timescale our weight appears to be very constant (as shown in Figure 1F, the weight is nearly flat for 2 years). Neumann noted constancy of his weight over more than a year, without conscious efforts to control food intake or expenditure (Neumann, 1902). The remarkable weight constancy was explained by Chow and Hall, who demonstrated the very slow dynamics of weight change, which effectively buffers fluctuations in bodily activity and food consumption (Chow and Hall, 2014). However, constancy is not the same as stability. To be stable, the weight has to return to the original value after a transient perturbation to a new value. If the new value is maintained without returning to the old, then the weight is not stable, even if it is very constant. Figure 1F gives an example of weight stability. Following an upward deflection (the red arrow), the weight returns to the original value (the first green arrow). Following a downward deflection (the blue arrow), the weight also returns to the original value (the second green arrow). In recent decades, many perturbation experiments have been performed, which all demonstrated weight stability (Sims and Horton, 1968;

[1]Department of Biology, Southern University of Science and Technology, Shenzhen, Guangdong 518055, China

[2]Guangdong Provincial Key Laboratory of Computational Science and Material Design, Shenzhen, Guangdong 518055, China

[3]Guangdong Provincial Key Laboratory of Cell Microenviroment and Disease Research, Shenzhen, Guangdong 518055, China

[4]Shenzhen Key Laboratory of Cell Microenviroment, Shenzhen, Guangdong 518055, China

[5]Lead Contact

*Correspondence: wanggy@sustech.edu.cn

https://doi.org/10.1016/j.isci.2020.101176

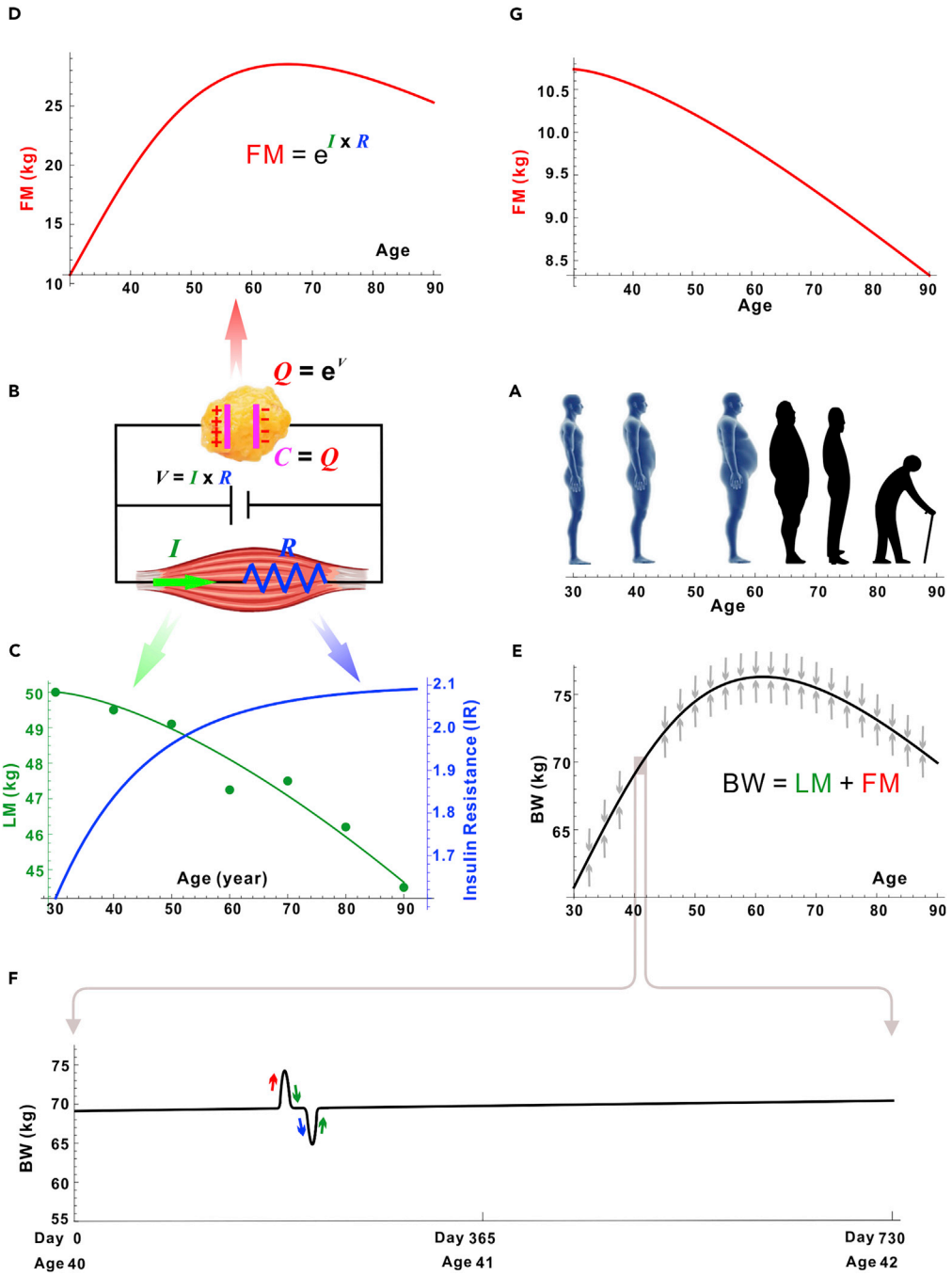

Figure 1. Body Mass Dynamics Governed by the Metabolic Ohm's Law

(A) From middle-age spread to old-age shrinkage.

(B) Electric circuit as an analogy to energy metabolism, where the lean (fat) tissue is analogous to a resistor (capacitor).

(C) The functions LM(Age) and IR(Age) are presented by the green and blue curves, respectively. LM(Age) is a decreasing function (Equation 13), analogous to the decreasing electric current in (B); IR(Age) is an increasing function (Equation 14), analogous to the increasing electric resistance in (B).

(D) FM(Age) was obtained by Equation 7 with LM(Age) and IR(Age) as input. Note that FM is analogous to the electric charge stored in the capacitor.

(E) BW(Age) obtained by Equation 8. The arrows indicate the stability of the trajectory.

Figure 1. *Continued*
(F) Extended view of BW(Age) with age ranging from 40 to 42 years (to scale). The trajectory is so flat that the slow weight gain may not be noticed. The spikes indicate perturbations that demonstrate weight stability.
(G) If peripheral insulin resistance remains constant (IR(Age) ≡ 1.60), fat is lost consistently.

Passmore, 1971; Salans et al., 1971; Mitchel and Keesey, 1977; Rothwell and Stock, 1979; Leibel and Hirsch, 1984; Leibel et al., 1995; Leibel, 2008; Ravussin et al., 2014; Rosenbaum and Leibel, 2016). Although the weight value can be perturbed away by persistent overfeeding or underfeeding, it always returns to its original value once normal feeding is reinstated. Our weight is therefore truly stable.

To explain weight stability, Kennedy proposed the lipostatic set-point theory (Kennedy, 1953), which has become a central tenet in metabolism: our body fat is under active regulation by the central nervous system (CNS). As a hormone secreted by adipocytes, leptin carries fat level information to the brain (Zhang et al., 1994). The signal is compared with a hypothetical "set-point" in the hypothalamus; and the difference acts as a feedback signal to modulate food intake and energy expenditure, thereby maintaining weight stability (Figure S2). Despite being textbook knowledge (Müller et al., 2018), the theory has serious problems: the nature of the neuronal set-point, including its existence, is unclear, and the roles played by leptin have been questioned (Leibel, 2008; Ravussin et al., 2018; Speakman, 2018a, 2018b; Zeng et al., 2015). See Supplemental Information for more information. We believe the lipostatic theory is afflicted by two misconceptions. The first misconception is that weight change is a sign of destabilization, i.e., weight change and weight stability are mutually exclusive. The second misconception is that weight stability is regulated by the CNS through leptin signaling. The two misconceptions together provoked the concept of leptin resistance, a putative pathologic condition of the brain (Frederich et al., 1995), to explain the mysterious middle-age spread. Unfortunately, the existence of leptin resistance has not been verified. In contrast, perturbation experiments have demonstrated strong weight stability under all the tested conditions—weight destabilization simply does not exist.

In this paper, we found that weight value change and weight stability are independent. On the one hand, body weight changes naturally, and the trajectory of weight change is governed by a metabolic Ohm's law (which will be summarized later by Equation 11). On the other hand, we found that the changing weight is actually stable, and the stability arises from each adipocyte's intrinsic self-tuning, which confers inertia on the body against deviating from the trajectory (Figure 1E, the gray arrows). Therefore, the weight is already stable even without regulation from the CNS. In summary, weight change and weight stability co-exist peacefully, just as the movement of a planet does not contradict the stability of the whole orbit. With this important decoupling, the main conundrums in the field would vanish when the fundamental assumptions of the present model are tested true. Middle-age spread is perhaps not a sign of destabilization but part of the natural trajectory of weight change, which conforms with all the perturbation experiments. Because weight stability is a peripheral autonomous and requires no central regulation, the applicability of the lipostatic theory, including the concept of leptin resistance, should be reconsidered.

If the brain has no intention to fix the fat storage, what is the biological function of the fat-leptin-hypothalamus axis? It might be simply to ensure a minimal fuel reserve for the lean tissues, as implied by the finding that leptin is physiologically important only at low concentrations and unimportant at normal to high concentrations (Perry et al., 2019). In addition to fat, whose level is conveyed by leptin, the other energy substrates are also monitored, including plasma glucose (whose level is conveyed by insulin) and even food in the stomach (whose amount is conveyed by the hormone ghrelin) (Figure S3B). Integration of these signals allows the hypothalamus to holistically perceive the body's total energy status and to evaluate a suitable appetite so that the lean tissues' energy demand can be met in a timely manner. A new paradigm, called leanocentrism, is formed.

Figure S1 presents a road map connecting different parts of this paper.

RESULTS

The Leanocentric Energy Balance

Because the body's energy expenditure is essentially for lean tissues, we have

$$E_{intoLean} = TEE, \qquad \text{(Equation 1)}$$

where $E_{intoLean}$ is the daily energy entry into the lean tissues and TEE is the total energy expenditure per day (Figure 2A). The energy is ultimately from food intake (EI), which enters both lean and fat tissues (Dulloo,

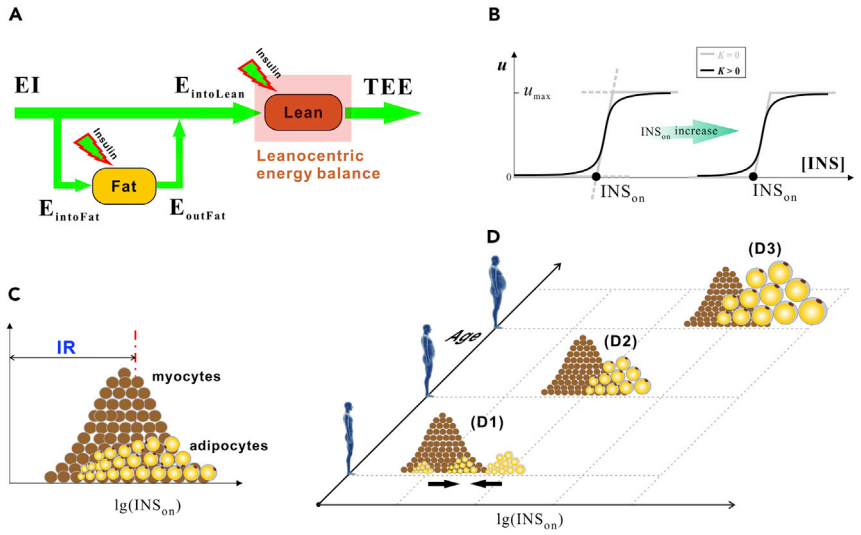

Figure 2. Leanocentric Energy Balance

(A) Leanocentric energy balance ($E_{intoLean}$ = TEE) is an overarching principle dominating body mass dynamics, including the conventional energy balance ($E_{intoFat}$ = E_{outFat}, or equivalently, EI = $E_{intoLean}$ = TEE).

(B) The insulin response curve u(INS). It is characterized by the threshold INS_{on}. As INS_{on} increases, the response shifts to the right.

(C) The distribution of myocytes and adipocytes over the lg(INS_{on}) axis.

(D) Explanation of middle-age spread. During aging, MD naturally shifts to the right, representing increased insulin resistance, which drags AD (being locked) in turn to the right, manifesting as a consistent increase in adipocyte size. (D1) explains a new mechanism of weight stability (fat mass homeostasis). AD can be perturbed to the right (left) by overfeeding (underfeeding). However, once normal feeding is reinstituted, it will gradually return to the locking point, indicated by the leftward (rightward) arrows.

2017). The fat tissues also release free fatty acids (FFAs) to nourish the lean tissues. If the energy flowing into the fat tissues equals that flowing out, then the conventional energy balance is established:

$$E_{intoFat} = E_{outFat}, \quad \text{(Equation 2)}$$

which is equivalent to (see Figure 2A)

$$EI = E_{intoLean} = TEE \quad \text{(Equation 3)}$$

In addition to Equations 2 and 3, the conventional energy balance can also be expressed by

$$FM \equiv \text{const.} \quad \text{(Equation 4)}$$

Note that conventional energy balance does not always hold. Energy imbalance (EI > TEE or EI < TEE) does occur occasionally.

We primarily consider a condition called *necessary feeding*; namely, EI is just sufficient for TEE. Note that this does not necessarily mean EI = TEE because under some conditions, EI has to be greater than TEE. For example, consider a man who has experienced prolonged starvation and is now allowed to eat freely. As a result of starvation, the adipocytes are very small and thus very insulin sensitive (see below); they thus preempt nutrient intake ($E_{intoFat}$ overly large), making $E_{intoLean}$ much smaller than EI. To fund the required TEE, EI must be far greater than TEE to make $E_{intoLean}$ equal TEE. This "overeating" necessity lasts for some days, during which FM gradually increases and EI gradually decreases, until finally FM returns to the prestarvation value and EI approaches TEE, signifying restoration of the conventional energy balance. This adaptive change in EI according to the prescribed TEE is called necessary feeding. By using necessary feeding with a suitable value of TEE, overnutrition is ruled out, whereby the natural tendency of weight gain can be highlighted.

The ODE Model

We developed an ODE model (Transparent Methods) to simulate the dynamics of plasma glucose (GLU), FFA, amino acids (AA), insulin (INS) concentrations, and the adipocyte masses m_i (i = 1, 2, …, N_{adipo}), where

N_{adipo} is the number of in silico adipocytes (Figures S4–S9). The model thus comprises (N_{adipo} + 4) ODEs and some algebraic equations. The value of N_{adipo} is chosen sufficiently small to make numerical simulations practical; thus, an *in silico* adipocyte represents a collection of many real adipocytes but not a single real adipocyte. In addition to the N_{adipo} in silico adipocytes, there are N_{myo} in silico myocytes (j = 1, 2, …, N_{myo}) in the model. Unlike in silico adipocytes, which are variables of the model, *in silico* myocytes are parameters of the model. Note that the subscripts i and j are used to number adipocytes and myocytes, respectively.

In the model, EI is in the form of meal ingestion, which prompts extensive changes in the concentration of the plasma nutrients and finally leads to their absorption by the body tissues, completing one meal cycle. By performing the simulation for three successive meal cycles, a day's system dynamics can be obtained. By performing the simulation for many days, a long-term system dynamics can be obtained.

For the parameter values of the model, most of them were obtained by fitting clinical data on plasma nutrient dynamics (Polonsky et al., 1988a, 1988b; Bonadonna et al., 1990, 1993; Havel et al., 1963; Stumvoll et al., 2000). These canonical values, presented in Table S1, were used by default in the simulations. That is, if a parameter's value is not mentioned for a simulation, then the canonical value was used. The two most important parameters, IR and TEE, being case dependent, were not assigned canonical values.

The validity of the computational model is suggested by the following: it is based on well-established principles; most of the canonical parameter values are taken from experimental measurements; and it can accurately predict the amount of weight change due to the change in TEE (Figure S10 and Table S4).

Cell Insulin Responses and Threshold Distributions

Insulin stimulus elicits a variety of responses in a cell (Quek et al., 2020), such as nutrient intake, suppression of proteolysis or lipolysis, and de novo lipogenesis. In this paper, insulin response refers specifically to nutrient intake. The response curve is denoted by u(INS) (Figure 2B), where u represents the cell's rate of nutrient intake and INS represents the plasma insulin concentration. The N_{myo} myocytes and N_{adipo} adipocytes compete for nutrients. That is, the growth of adipocyte i depends not only on its own insulin response u_i(INS) but also on the myocytes' insulin response: u_j(INS) (j = 1, 2, …, N_{myo}), as well as the responses of other adipocytes.

Biochemical responses often follow a threshold mechanism (Goldbeter and Wolpert, 1990), which applies to insulin response (Wang, 2010, 2012; Li and Wang, 2014). In this paper, the insulin response u(INS) is a sigmoidal curve characterized by a response threshold INS_{on} (Figure 2B), which can be used to quantify the cell's insulin resistance. Indeed, the larger the threshold, the more difficult it is for the cell to respond, that is, the more resistant the cell is to insulin. In this paper, we used lg(INS_{on}) to quantify a cell's insulin resistance because the biochemical dose response is conventionally plotted on the log scale, including the insulin dose response (Bonadonna et al., 1990; Bedinger et al., 2015; Cieniewicz et al., 2017). Each insulin-responsive cell has its own lg(INS_{on}) value. By fitting the clinical data in (Bonadonna et al., 1990), we found that the cell lg(INS_{on}) values form a roughly normal distribution (Wang, 2014). The mean of the distribution, denoted by IR, is used to quantify the overall peripheral insulin resistance. Here, the myocyte and adipocyte distributions are considered separately, as a myocyte distribution (MD) and an adipocyte distribution (AD) (Figure 2C). Because muscle is the main insulin-responsive tissue, the mean of MD should be very close to IR. Therefore, the MD is simply denoted by (IR, σ_{myo}), where σ_{myo} is the standard deviation. AD is denoted by (μ_{adipo}, σ_{adipo}).

A simulation result can be partly represented by the evolution of AD. In Figure 3A3, for example, the AD evolves as a part of the whole system's dynamics, starting from the initial blue distribution (arbitrarily given) and finally stabilizing at the yellow distribution. It will turn out that the location of the yellow distribution is largely determined by the MD (the brown distribution). In other words, the AD is finally locked by the MD, and the "blue to yellow" evolution can be regarded as the return of AD to the locking point. See also the rightward arrow in Figure 2D1. Similarly, if AD is initially perturbed to the right, then the subsequent evolution will be toward the left, indicated by the leftward arrow in Figure 2D1. Regardless of how AD is perturbed, it will finally return to the locking point, demonstrating weight stability. The above scenarios are under the condition that MD is fixed. In reality, MD shifts to the right very slowly (see below), which drags AD to the right very slowly (Figures 2D1–D3). Because adipocyte insulin resistance positively correlates with

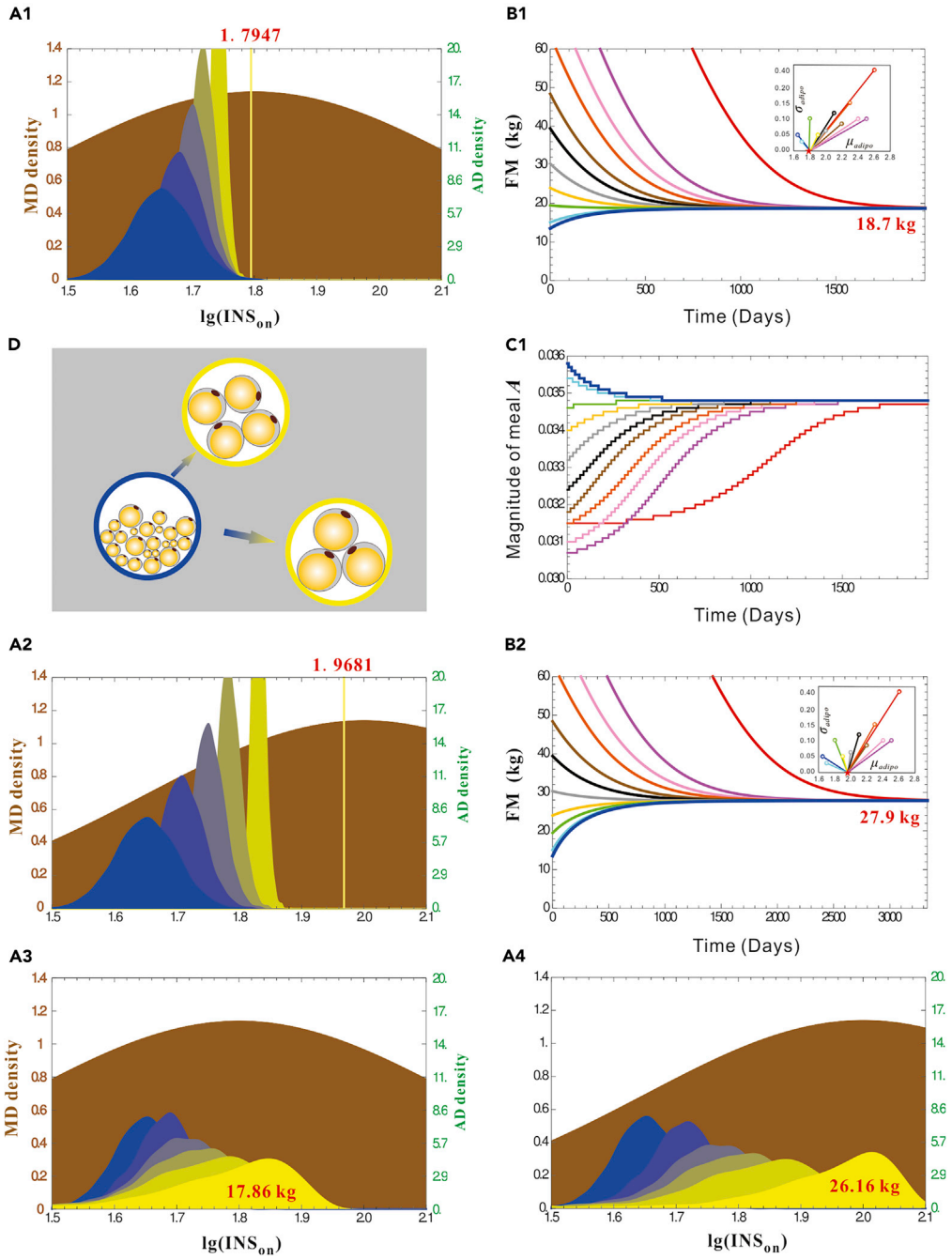

Figure 3. Stabilization of Adipocytes

(A1) The MD (1.80, σ_{myo}), indicated by brown, was fixed. The initial AD (1.65, 0.05) is indicated by blue. The AD evolved and finally stabilized at lg(INS$_{on}$) = 1.7947 (the yellow spike). (B1) Eleven FM(t), corresponding to 11 initial ADs as indicated by the 11 dots in the inset. (C1) The magnitude of meal supply A (see Equation S13) as a function of time. Each color corresponds to the same color in B1. (A2) The MD (2.00, σ_{myo}) was fixed. The initial AD (1.65, 0.05) evolved and finally stabilized at an elevated value lg(INS$_{on}$) = 1.9681 (the yellow spike). (B2) Eleven FM(t), corresponding to IR = 2.00, and 11 initial ADs as indicated by the 11 dots in the inset. (D) Indication of the initial and final sizes of adipocytes. (A3) Same as A1 (IR = 1.80) but with randomized u_{max}. That is, the maximum rate of nutrient intake u_{max} is different for different cells. (A4) Same as A3 except IR = 2.00.

adipocyte size (Salans et al., 1968; Engfeldt and Arner, 1987; Guilherme et al., 2008; Yang et al., 2012), the right-shift of AD manifests as persistent weight gain, namely, middle-age spread.

Weight Is Stable in the Absence of Central Regulation

To test weight stability using the ODE model, one can start with adipocytes of arbitrary masses, which would evolve as a part of the whole system's dynamics. If the masses finally stabilize, then weight stability is demonstrated. The following simulations reproduce weight stability. The stability is independent of lipostatic regulation because the model does not have such a component.

Consider a subject with TEE = 2,400 kcal/day and MD of (IR, σ_{myo}) = (1.80, 0.35) (Figure 3A1, brown). Let the simulation start with an initial AD of (μ_{adipo}, σ_{adipo}) = (1.65, 0.05) (Figure 3A1, blue), corresponding to an initial FM of 13.4 kg. The AD shifted to the right and narrowed at the same time until all the adipocytes stabilized at the same lg(INS_{on}) value of 1.7947 (the yellow spike) or at the same mass m_i = 0.00935 kg. Therefore, FM increased over time and finally stabilized at 0.00935 × N_{adipo} = 18.7 kg (Figure 3B1, the blue curve). Meanwhile, the food amount decreased over time and finally stabilized (Figure 3C1, the blue curve). This was an expected result under necessary feeding. The adipocytes were very small initially, signifying the body's energy deficit; thus, the initial "overeating" (EI > TEE) was necessary.

The simulation was repeated ten times, each with a new initial AD. The 11 initial ADs are represented by the 11 dots of (μ_{adipo}, σ_{adipo}) in the inset of Figure 3B1. The colored dots correspond to the curves of the same color in Figures 3B1 and 3C1. The final FM was always 18.7 kg, corresponding to lg(INS_{on}) = 1.7947 for every adipocyte (the yellow spike in Figure 3A1).

Peripheral Insulin Resistance Is a Determinant of Weight

To learn muscles' influence on FM, we started the simulation with the same 11 initial ADs but with MD shifted to the right (IR, σ_{myo}) = (2.00, 0.35) (Figure 3A2, brown), which means that the muscle is more insulin resistant. The resultant functions FM(t) are presented in Figure 3B2. Compared with their IR = 1.80 counterparts, the primary difference was that the steady FM rose from 18.7 to 27.9. That is, every adipocyte's lg(INS_{on}) increased from 1.7947 to 1.9681 (Figure 3A2, the yellow spike). Together with Figures 3A3 and 3A4 (see below), the results demonstrate that insulin resistance is a determinant of the weight value: AD is "locked" by MD. As MD moves to the right, AD moves concomitantly, and the adipocytes become larger (weight gain). This new mechanism is called the *leanocentric locking-point model*.

The model can explain the "environment-dictated adipocyte growth" phenomenon revealed by Ashwell et al., who transplanted adipocytes into recipient mice and found that the donor adipocytes always tune their size to that of the recipient adipocytes (Ashwell et al., 1977). They concluded that the local environment of the transplantation site is important, but they did not know the determinant. Now, the puzzle is solved. As the yellow spikes in Figures 3A1 and 3A2 demonstrate, the final adipocyte sizes are determined by the recipient's peripheral insulin resistance, which is indeed an environmental factor around the graft. Therefore, the data of Ashwell et al. are consistent with the locking-point model, which in turn provides unique insights into the interpretation of the data.

Weight Stability Is a Cell-Autonomous Property of Adipocytes

In the absence of lipostatic regulation, what causes FM homeostasis? A clue to the answer is that the adipocytes always grew to the same size eventually, no matter how different they had been to start with. This phenomenon suggests the adaptive growth of adipocytes: smaller (larger) ones grow faster (slower); thus, all the cells eventually reach the same size. Adaptive growth might be rooted in the positive correlation between an adipocyte's insulin resistance and its mass (Salans et al., 1968; Engfeldt and Arner, 1987; Guilherme et al., 2008; Yang et al., 2012). A large adipocyte is insulin resistant; thus, it usually absorbs too few nutrients to sustain itself, and the cell gradually shrinks. A small adipocyte is insulin sensitive; thus, it usually absorbs more nutrients than it actually needs, and the cell grows. Therefore, an adipocyte settles at a medium mass due to the self-tuning of insulin resistance.

The homogeneity of adipocytes, although a great indicator of self-tuning, is not quite realistic, because adipocytes should have certain heterogeneity in size (Stecco, 2014). The heterogeneity may originate from differential growth conditions. For example, cells in the vicinity of arteries are exposed to higher concentrations of nutrients and insulin and thus grow more than those in the vicinity of distal capillaries. The

differential growth may counteract adaptivity and lead to a certain degree of heterogeneity. To test this idea, the maximal rate of nutrient intake u_{max}, which had been a constant, was randomized with a normal distribution (μ_{umax}, σ_{umax}). With this change, AD evolved and finally stabilized at the yellow distribution (Figures 3A3 or 3A4 for IR = 1.80 or 2.00, respectively). The distributions were wide, corresponding to relatively heterogeneous adipocytes. The total FM was only slightly different from the case of constant u_{max} (17.86 versus 18.7 and 26.16 versus 27.9).

With heterogeneity now taken into account, FM homeostasis can be understood as the fixation of AD by MD. In Figure 2D1, the middle AD corresponds to the locked FM. It can be transiently perturbed to the right by overfeeding (the corresponding adipocytes become larger). However, once normal feeding is reinstituted, it will gradually return to the original position, as indicated by the leftward arrow. On the other hand, the middle AD can be transiently perturbed to the left by underfeeding (the corresponding adipocytes become smaller). However, once normal feeding is reinstituted, it will gradually return to the original position, as indicated by the rightward arrow. By adaptively tuning their insulin resistance, the adipocytes have acquired some inertia against deviation from the locking point. Because the CNS is not involved, weight stability is a cell-autonomous property of adipocytes.

The following simulations were all based on the randomized u_{max} with the normal distribution (μ_{umax}, σ_{umax}).

Middle-Age Spread Is Almost Irresistible

The simulations have demonstrated that insulin resistance promotes weight gain. The reverse, namely, weight gain promotes insulin resistance, has long been known (Guilherme et al., 2008; Kim et al., 2018b; Kita et al., 2019). As body fat increases, insulin signaling is more blunted by increased FFA levels, exacerbating insulin resistance. Therefore, weight gain and insulin resistance aggravate each other, forming a self-perpetuating circle (positive feedback loop). The loop does not define the direction of change: both automatic weight gain and automatic weight loss are possible consequences of the positive feedback. Indeed, fat loss enhances insulin sensitivity, and the enhanced insulin sensitivity reduces fat further; thus, the positive feedback can also lead to automatic weight loss. Why, then, is only weight gain automatic in reality? The reason might be that IR tends to increase during aging for many reasons, including aging-related increase of S-nitrosation in the insulin signaling pathway (Ropelle et al., 2013; Pearson et al., 2015). This natural tendency causes the direction of weight change (Figure 2D). Although measures such as exercises may reduce insulin resistance, the effects are temporary and die out rapidly. Middle-age spread is thus a natural manifestation of aging.

The aging-related IR aggravation is obviously a hypothesis of fundamental importance. The hypothesis is supported by some early studies. Ropelle et al. found that aging increases inducible nitric oxide synthase expression and S-nitrosation of major proteins involved in insulin signaling, thereby reducing insulin sensitivity in mouse skeletal muscle (Ropelle et al., 2013). Fink et al. measured the degree of insulin resistance of 27 non-elderly (mean age 37 $\pm$ 2) and 17 elderly (mean age 69 $\pm$ 1) subjects, who were all healthy, non-obese, and leading active lives (Fink et al., 1983). Although the difference in body adiposity was small between the non-elderly and elderly groups (body mass index [BMI]: 23 versus 24; relative body weight [RBW]: 0.94 versus 0.93), their difference in insulin resistance, quantified by glucose disposal rate, was striking (247 $\pm$ 12 versus 151 $\pm$ 17 $mg \times m^{-2} \times min^{-1}$). Having these evidences notwithstanding, the hypothesis needs to be further tested by more rigorous experiments. Indeed, the latter evidence can be questioned because BMI and RBW may not be good indicators of adiposity. The experiment can be re-performed in the future by using bioimpedance analysis (BIA) or dual energy X-ray absorptiometry (DXA) to obtain more accurate adiposity measurement.

The LM-IR-FM Equation

In the ODE modeling, the parameters are fixed at their canonical values except TEE and IR, which do not have canonical values. Therefore, given a (TEE, IR) pair, the ODE model computes the corresponding steady FM. This raises the possibility of obtaining an algebraic relationship among the triad (TEE, IR, FM) by integrating the ODE model with sufficient clinical data. We actually replaced TEE with LM because the two are roughly proportional (see Equation (c) in Figure 6C and its explanation in the caption). LM is better suited to the equation because it is intrinsic to the body, as are IR and FM, whereas TEE is extrinsic. The equation is called the LM-IR-FM equation (LIFE).

To derive LIFE, we started from a rough estimation of IR. Because MD and AD are interlocked, IR should be close to the mean of AD (Figure 2C). Together with a further simplification that all the adipocytes are identical, we have

$$IR \approx \lg(INS_{on})_i = \lg\frac{m_i}{\xi} \approx \lg\frac{FM}{\xi \times N_{adipo}}.$$

Note that we have used Equation S10, namely $(INS_{on})_i = m_i/\xi$, which models the positive correlation between m_i and $(INS_{on})_i$ (Salans et al., 1968; Engfeldt and Arner, 1987; Guilherme et al., 2008; Yang et al., 2012). Substituting $\xi = 1.5\times10^{-4}$ and $N_{adipo} = 2000$ (Table S1) into the above equation, we obtain

$$IR \approx 0.523 + \lg(FM) \quad \text{(Equation 5)}$$

To bring LM into the equation, note that LM should negatively correlate with IR. Intuitively, a more muscular man (LM larger) should be more insulin sensitive (IR smaller), thus the negative correlation. The underlying molecular mechanism is as follows: the more myocytes are in the body, the less ectopic fat deposition per myocyte and the more insulin sensitive the myocyte. To embody the negative correlation and conform with Equation 5, LIFE was designed as

$$IR = \gamma_0 + \gamma_1\frac{\lg(FM)}{LM - \gamma_2} \quad \text{(Equation 6)}$$

To estimate the unknown parameters γ_0, γ_1, and γ_2, we collected clinical data on 44 subjects from the literature (Table S3). Each subject actually represents a group of people whose data were averaged in the original literature. By the estimation procedure described in Transparent Methods, we obtained $\gamma_0 = 0.664$, $\gamma_1 = 45.4$, and $\gamma_2 = 0$, with which Equation 6 can be presented as the straight line in Figure 4A. LIFE is also expressed in terms of the solution to FM:

$$FM = \exp\left(\frac{\ln 10 \times LM \times (IR - \gamma_0)}{\gamma_1}\right), \quad \text{(Equation 7)}$$

whereby the body weight is determined:

$$BW = LM + \exp\left(\frac{\ln 10 \times LM \times (IR - \gamma_0)}{\gamma_1}\right) \quad \text{(Equation 8)}$$

LIFE Is a Better Health Indicator Than Body Mass Index

The 44 subjects in Table S3 were diverse, spanning from very thin (FM = 6.6 kg) to very fat (FM = 68.0 kg). Among them, 12 were athletes. They were classified according to BMI as normal weight, overweight, and obese. Their lg(FM)/LM and IR values are presented as the *x* and *y* coordinates, respectively, of the 44 dots in Figure 4A. There were six outliers whose data did not scatter around the regression line. In Transparent Methods, we explain why they were outliers. Note that the six outliers were excluded from estimating γ_0, γ_1, and γ_2.

For the 38 nonoutliers, those located toward the lower left should be healthier. The athletes' IR values were near or below 1.5, whereas those of nonathletes generally ranged from 1.5 to 2.2. The four obese subjects were obviously unhealthy. The other weight categories were quite heterogeneous. The normal weight subjects scatter widely along the regression line, suggesting that normal weight does not correspond to normal health. For example, subject 18 (BMI = 24.9) might appear to be normal, but he or she was very insulin resistant, with an IR as high as those of the obese subjects. Overweight subjects are also widely scattered. Subject 39, although overweight, was actually healthy, with an IR value as small as those of some athletes. These results demonstrated that BMI is not a good health indicator. Interestingly, comparative analysis of FM measurement and BMI on the US 1999–2004 National Health and Nutrition Examination Survey (NHANES) data reached almost the same conclusion: a considerable proportion of subjects in the healthy BMI range 20–25 were found to have excess adiposity, whereas BMI >30 reliably defines obesity regardless of age and sex (Dybala et al., 2019).

Therefore, LIFE (Equation 6) provides a much better health indicator, namely, the body's peripheral insulin resistance computed from the body composition (LM and FM), which can be easily measured by methods such as BIA and dual-energy DXA.

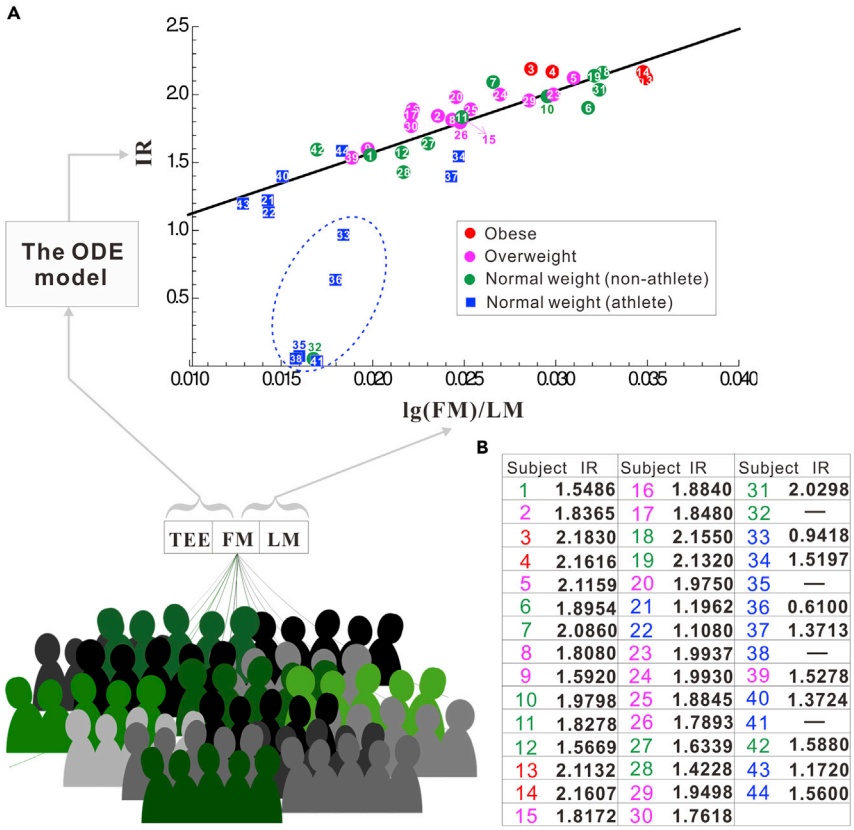

Subject	IR	Subject	IR	Subject	IR
1	1.5486	16	1.8840	31	2.0298
2	1.8365	17	1.8480	32	—
3	2.1830	18	2.1550	33	0.9418
4	2.1616	19	2.1320	34	1.5197
5	2.1159	20	1.9750	35	—
6	1.8954	21	1.1962	36	0.6100
7	2.0860	22	1.1080	37	1.3713
8	1.8080	23	1.9937	38	—
9	1.5920	24	1.9930	39	1.5278
10	1.9798	25	1.8845	40	1.3724
11	1.8278	26	1.7893	41	—
12	1.5669	27	1.6339	42	1.5880
13	2.1132	28	1.4228	43	1.1720
14	2.1607	29	1.9498	44	1.5600
15	1.8172	30	1.7618		

Figure 4. Discovery of LIFE

(A) A scatterplot of 44 subjects' lg(FM)/LM (the *x* axis) and IR (the *y* axis). The latter was computed by the ODE model based on the subjects' clinical data, especially TEE and FM. Regression analysis revealed a linear relationship between lg(FM)/LM and IR. The six subjects within the oval were outliers.

(B) The obtained IR values of the 44 subjects.

LIFE Explains Forbes' Data

LIFE can be expressed in terms of the solution to LM:

$$LM = \frac{\gamma_1}{IR - \gamma_0} lg(FM) \qquad \text{(Equation 9)}$$

It is similar to an empirical formula relating FM to LM, namely, Forbes' formula:

$$LM = 23.9lg(FM) + 14.2, \qquad \text{(Equation 10)}$$

which was discovered by the examination of FM and LM in six groups of subjects (Forbes, 2000, 2012). By presenting every group's average (FM, LM) as a dot in Figure 5A, Forbes found that these cross-sectional data can be well fitted by the dashed curve in Figure 5A, namely, the Forbes formula. The formula implies a positive correlation between LM and FM, which is unfortunately not applicable to the longitudinal body change of an ordinary middle-aged person, who is losing LM (sarcopenia) and gaining FM, resulting in a negative correlation between LM and FM. This puzzle is now resolved by Equation 9, which contains in the denominator the critical factor IR, whose slow increase counteracts the increase in FM (which is in the numerator) and allows the slight decrease in LM, thus enabling the longitudinal negative correlation between FM and LM.

LIFE fits with the six data best at IR = 2.0061 (Figure 5A, the red curve). This good but imperfect fitting is expected. With a fixed IR, LIFE describes a single person at a single time, which of course cannot fit perfectly with the data of six subjects whose IRs were all different. IR = 2.0061 should be some medium value among the six IRs, which is indeed the case (Figure 5B).

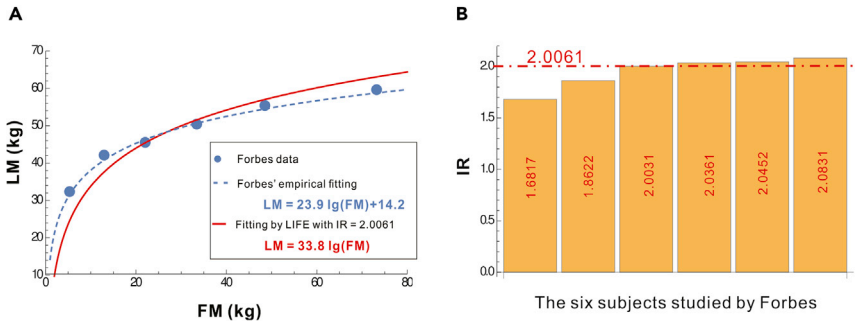

Figure 5. LIFE Explains Forbes' Data

(A) Forbes' cross-sectional data reveal that LM is a logarithmic function of FM. The dots represent clinical data collected by Forbes. The dashed curve is an empirical fitting by Forbes. The solid curve is a fitting by LIFE.

(B) The bars represent IR values of the six subjects, estimated by substituting their (FM, LM) into Equation 6.

The Metabolic Ohm's Law

Equation 7 can be converted into

$$\begin{cases} V = I \times R \\ Q = e^{V} \end{cases} \qquad \text{(Equation 11)}$$

by the substitutions $I = \ln 10 \times \mathrm{LM}/\gamma_1$, $R = \mathrm{IR} - \gamma_0$, $Q = \mathrm{FM}$, and using a new variable V. Equation 11 is analogous to a resistor and capacitor connected in parallel, with I, R, V, and Q being the electric current, resistance, voltage, and charge, respectively (Figure 1B). The analogy is pertinent. The lean tissue, which primarily expends energy, is analogous to a power-dissipating resistor. The fat tissue, which primarily stores energy, is analogous to a power-storing capacitor. Quantitatively, FM measures the stored energy and is perfectly analogous to the stored electricity ($Q = \mathrm{FM}$); the peripheral insulin resistance is naturally analogous to the electric resistance ($R = \mathrm{IR} - \gamma_0$); the analogy $I = \ln 10 \times \mathrm{LM}/\gamma_1$ is easy to understand because LM is proportional to TEE, which, as the energy current through the lean tissue, is perfectly analogous to the electric current through the resistor.

In Equation 11, the first equation $V = I \times R$ is Ohm's law of the body's fuel metabolism; the second equation $Q = e^{V}$ implies that the capacitor is not a regular one with a constant capacitance but a nonlinear one with a capacitance equaling the stored charge: $C = \mathrm{d}Q/\mathrm{d}V = Q$. In other words, the more the capacitor is charged, the larger its capacity of further charging. The self-perpetuating capacitor may originate from the self-perpetuating circle between weight gain and insulin resistance. It has already explained why individuals with higher body fat have higher fat gains. More importantly, it is easy to predict how much more the person with more fat will gain.

Ohm's Law Predicts How Much More the Person with More Body Fat Gains

A middle-aged person gains weight much more easily than a younger person. As usual, the middle-aged person has more body fat ($Q_y < Q_m$; or $C_y < C_m$) and higher insulin resistance ($R_y < R_m$). Here, the subscripts y and m represent young and middle aged, respectively. Now let the two increase their regular EI by the same small amount $d\mathrm{EI}$, i.e., $dI_y = dI_m$ (Figure 6A1). The same condition leads to different outcomes due to two levels of differentiation. The resistance difference $R_y < R_m$ makes $dI_y \times R_y < dI_m \times R_m$, namely, $dV_y < dV_m$ (Figure 6A2). The capacitance difference $C_y < C_m$ further amplifies the effect $C_y dV_y << C_m dV_m$, namely, $dQ_y << dQ_m$ (Figure 6A3), indicating that the person with more body fat gains much more fat.

The analytical expression of $\mathrm{d}Q$ was obtained in Transparent Methods:

$$d\mathrm{FM} = \frac{\mathrm{FM} \times \ln \mathrm{FM} \times d\mathrm{EI}}{\sigma_1 \times \mathrm{PAL} \times \mathrm{LM}}, \qquad \text{(Equation 12)}$$

where σ_1 and PAL (physical activity level) are explained in the caption of Figure 6C. Equation 12 predicts how much more the person with more body fat gains. It shows that $d\mathrm{FM}$ scales as $\mathrm{FM} \times \ln \mathrm{FM}$, even faster than the linear scaling (Figure 6B). For example, a young person with 50 kg of LM and 10 kg of FM gains only 0.64 kg fat by eating 50 kcal more every day, whereas a middle-aged person with 50 kg of LM and

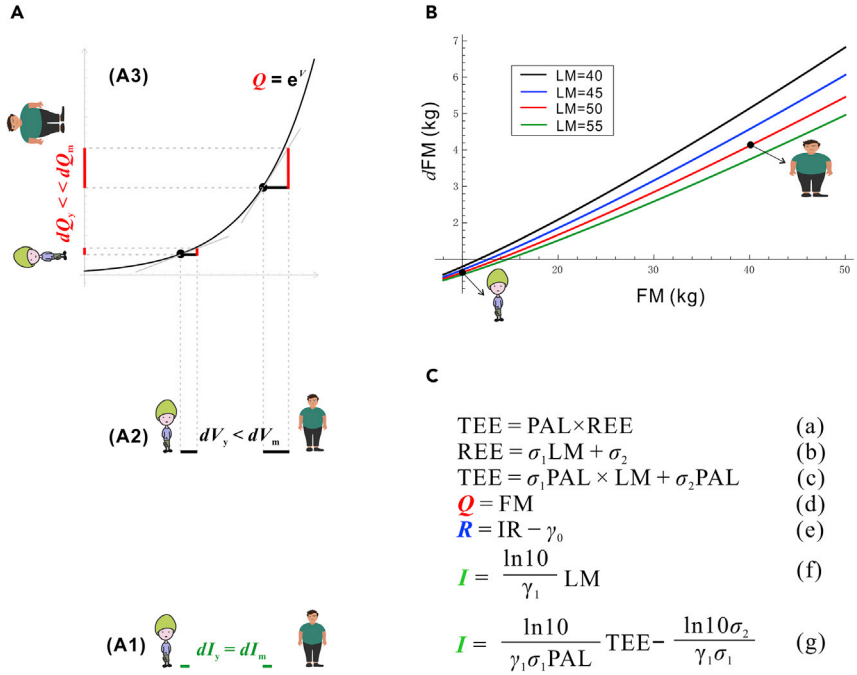

Figure 6. Metabolic Ohm's Law

(A) A schematic diagram explaining why individuals with more body fat also gain more fat.

(B) The fat gain *d*FM as a function of FM resulting from a regular increase in food amount *d*EI = 50 kcal/day, with PAL = 1.5.

(C) Main equations of the metabolic-electric analogy, where REE represents "resting energy expenditure"; PAL represents "physical activity level," which is the ratio of TEE and REE (Equation a). PAL is usually between 1.4 and 1.7 for a sedentary adult. Equation b is taken from (Creasy et al., 2018), where σ_1 = 23.9 kcal/(day×kg) and σ_2 = 372 kcal/day. Equation c is the combination of Equations a and b.

40 kg of FM gains 4.1 kg of fat, approximately 6.4-fold more than the young person. Importantly, the predictions are not difficult to test because the few parameters can be easily controlled or readily measured in clinical practice. This will help to validate and optimize Ohm's law.

Ohm's Law Governs Weight Change

Middle-age spread does not usually continue into very old age. People in the last century mostly started to lose weight at approximately 55–60 years of age (Williamson, 1993; Seidell and Visscher, 2000). Assume that *R* is always increasing. Then, according to Ohm's law, the only way to slow down weight gain is to decrease *I* (i.e., the loss of LM, primarily due to sarcopenia), and the decrease has to accelerate to lead to weight loss. Indeed, it was discovered that sarcopenia is a progressive process involving the accelerated loss of muscle mass and function (Cruz-Jentoft and Sayer, 2019). According to the Baltimore Longitudinal Study of Aging (BLSA) (Metter et al., 1999; Ferrucci et al., 2012), the annual rate of muscle loss is approximately 1%, 5%, and more than 10% by ages 40, 60, and 90 years, respectively (Figure 1C, the green dots). Note that the LM loss contributes to weight loss not only by itself but also by driving the reduction in FM (Equation 7). Therefore, the transition from weight gain to weight loss will occur sooner or later, as long as the subject lives sufficiently long (Figure 1A).

To test this idea, we first obtained LM as a function of age (Figure 1C, the green curve):

$$LM(Age) = LM_{30}\left[1 - 0.00023(Age - 30)^{1.5}\right] \quad \text{(Equation 13)}$$

by fitting the BLSA sarcopenia data. According to the locking-point theory, peripheral insulin resistance increases consistently during aging; thus, IR(Age) is an increasing function. Here, we assumed that IR has an upper bound IR_{max}; thus, the increase in IR slows down gradually, which can be readily modeled by a simple ODE $dIR/dAge = (IR_{max} - IR)/T_{half}$, where T_{half} is the half-maximum time starting from age 30 years. That is, T_{half} +30 is the age at which IR reaches $(IR_{max} + IR_{30})/2$, where IR_{30} is the IR at age 30 years. The simple ODE has an explicit solution:

$$IR(Age) = IR_{max} - (IR_{max} - IR_{30})\exp\left(\frac{30 - Age}{T_{half}}\right) \quad \text{(Equation 14)}$$

We let $IR_{30} = 1.60$ and $IR_{max} = 2.10$. This choice was inspired by Figure 4A, which shows that IR < 1.50 and IR > 2.20 are generally applicable to athletes and morbidly obese people, respectively; thus, the normal IR range should be close to (1.60, 2.10). By using $T_{half} = 15$ in Equation 14, the function IR(Age) was drawn as the blue curve in Figure 1C. By Equations 7 and 8, the functions FM(Age) and BW(Age) were obtained and presented in Figures 1D and 1E, respectively. The body weight peaks at age 61 years, which conforms well with the statistics (Williamson, 1993; Seidell and Visscher, 2000). To see how the results vary with T_{half}, we repeated the computations with T_{half} ranging from 10 to 25 years and found that the age of peak weight ranges from 56 to 66 years, which are all reasonable ages of transition from weight gain to weight loss.

The Remarkable Energy Resistor

We have demonstrated the paramount importance of peripheral insulin resistance in energy metabolism. At the least, it governs both aspects of body mass dynamics: weight stability is achieved by the adipocytes' self-tuning of their respective insulin resistance, and weight is dominated by the body's overall insulin resistance. Although the former (conferring stability) is certainly of merit, the biological significance of the latter is unclear.

We argue that the self-perpetuating circle of insulin resistance and weight gain is beneficial for long-term body protection. If our insulin resistance remained constant throughout, then our body fat would decline as sarcopenia progresses (Figure 1G, obtained with IR(Age) ≡ 1.6 and the LM(Age) expressed by Equation 13); body weight would then decline even more. The diminishing body mass would make it increasingly difficult for elderly people to deal with emergent situations such as acute diseases, accidents, and calamities, especially in ancient times. The aggravation of insulin resistance allows automatic fat accumulation even under necessary feeding to address the potential dangers in old age. Therefore, moderate middle-age spread is not rooted in hypothalamus defects that cause central leptin resistance (as proposed by the lipostatic theory) but is a healthy natural process.

In addition to this long-term protection, peripheral insulin resistance offers immediate and indispensable life protection by sparing glucose for the brain while the plasma glucose level is low (Neel, 1962; Wang, 2014). Peripheral insulin resistance, despite being the molecular mechanism underlying type 2 diabetes (Kahn, 1994), also plays critical roles in the body's fuel metabolism.

DISCUSSION

From Lipocentrism to Leanocentrism

Body mass dynamics are traditionally considered from a lipocentric perspective, which emphasizes leptin-mediated central feedback regulation on body fat (Figure S3A). Besides the lipostatic set-point model, there are other lipocentric models, such as the "two intervention point" (Herman and Polivy, 1983; Speakman, 2018a, 2018b) and "settling point" (Wirtshafter and Davis, 1977), which are less popular and have various problems (Supplemental Information). Despite dominance of the lipocentric view, the strong influence of LM on FM has long been recognized (Edholm et al., 1955; Lissner et al., 1989; Dulloo et al., 2017; Blundell et al., 2015). These works advocated the concept of LM homeostasis (protein-stasis), which works in parallel with FM homeostasis (lipostasis) to maintain the stability of both LM and FM, thus demonstrating a broader view (MacLean et al., 2017). However, neither of the two homeostatic mechanisms has been proven. Unlike the previous works that all focused on the *matter stored in* the tissues, this work focused on the *energy flowing through* the tissues, which led to the leanocentric locking-point model to compete with the existing models.

The Brain Only Has Limited Influence upon Body Weight

What afflicts the previous models is the rather intuitive perception that weight stability and weight value change are mutually exclusive: the former (latter) is normal (abnormal). Here, Ohm's law has led to the surprising discovery that the two are independent and can thus be decoupled.

The weight value, as a steady state of the ODE model, is determined by the model parameters. Table S2 shows how FM changes with changes in TEE/EI, IR, σ_{umax}, and N_{adipo}. Because most of the parameters change randomly without a bias, the resultant FM change is negligible because the slow dynamics can effectively buffer fluctuations (Chow and Hall, 2014). Interestingly, only TEE (analogous to I) and IR (analogous to R) change with a bias: the former (latter) generally decreases (increases), which generates a parabolic trajectory of weight change. Because TEE and IR are analogous to I and R, respectively, and their

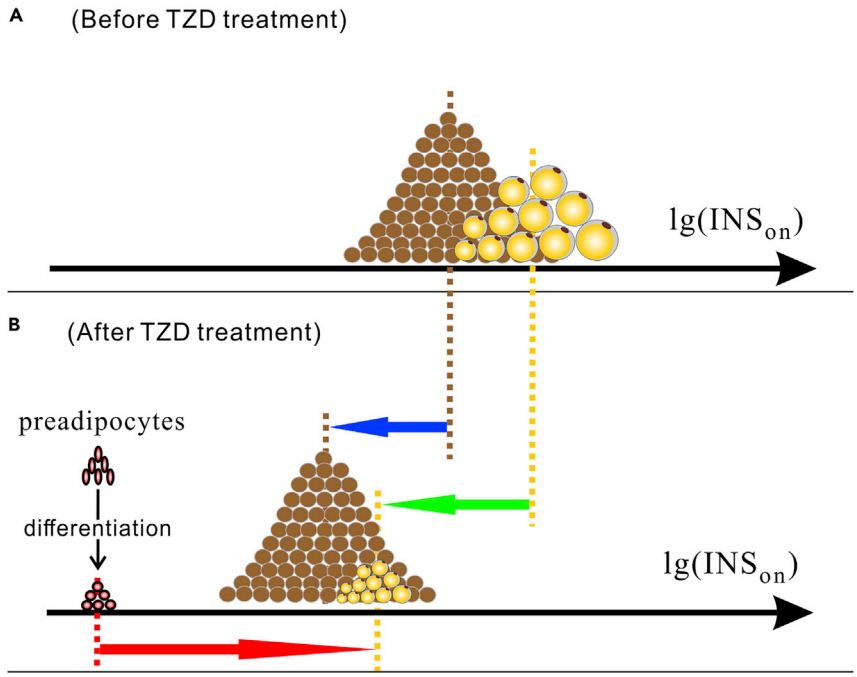

Figure 7. Scenarios Induced by TZD Treatment

(A) MD and AD before TZD treatment.

(B) After TZD treatment, MD moves to the left (the blue arrow), showing the insulin sensitization effect of TZD. The original adipocytes also move to the left (the green arrow) to satisfy the leanocentric principle. However, new adipocytes must be generated to account for the increased weight (the red arrow).

combined effect is quantitatively their product ($I \times R$), Ohm's law is clearly in action. Note that both parameters change so slowly that our weight value appears to be constant for years (Figure 1F).

Weight stability, in this view, is due to adipocytes' adaptive tuning of their insulin resistance, which confers some inertia against leaving the locking point; it is therefore a largely cell-autonomous property of adipocytes. Because leptin is physiologically effective only at low concentrations and unimportant at normal to high concentrations (Perry et al., 2019), leptin signaling just effects to avoid an extremely low adiposity; thus, the central regulation does not intend to fix any weight value by conferring stability properties.

Insights on Thiazolidinedione Treatment

The above discussion on parameters helps to resolve a puzzle about thiazolidinedione (TZD), a class of insulin-sensitizing drugs. The drugs enhance insulin sensitivity; thus, according to the present theory, they should reduce body weight, but they are well known as weight boosters. This puzzle is actually easy to resolve considering that TZD is multifactorial: it not only enhances insulin sensitivity but also increases the number of adipocytes (N_{adipo}) by promoting preadipocyte differentiation (Tang et al., 2011). Because the increase in N_{adipo} causes weight gain (Table S2), the concurrence of insulin sensitization and weight gain can be explained by the locking-point model provided that the increase in the number of adipocytes more than balances the decrease in the size of the adipocytes.

Remarkably, starting from the leanocentric principle, one can correctly predict the scenarios induced by TZD. In other words, TZD-induced adipose tissue remodeling, particularly preadipocyte differentiation, is largely an inevitable consequence of the locking-point model. Figure 7A indicates the original MD and AD. After the TZD treatment, the MD moves leftward (the blue arrow in Figure 7B) due to insulin sensitization. According to the locking-point model, the AD, being locked, also shifts to the left (the green arrow), and the adipocytes become smaller. Now that the adipocytes are shrinking, why does the weight increase instead? There must be massive numbers of new adipocytes generated (preadipocyte differentiation). The new adipocytes grow increasingly large (the red arrow); the original adipocytes become increasingly small (the green arrow); and finally, the two groups become indistinguishable. Due to the left-shifted MD, the final adipocytes are generally smaller than those before TZD treatment. Therefore, the increase in N_{adipo} has to be large to cause weight gain;

otherwise, the weight may still decrease. These predictions conform well with experimental observations (de Souza et al., 2001; Tang et al., 2011; Kim et al., 2018a). de Souza et al. (2001) found that TZD treatment led to "the shrinkage and/or disappearance of existing mature adipocytes," which corresponds to the green arrow in Figure 7B. On the other hand, the study by Tang et al. (2011) indicated that "TZDs roughly double the number of adipocytes formed during treatment, compared with controls"; Evans-Molina (2011) pointed out that "TZD-associated weight gain has been mostly attributed to the formation of new fat cells."

Ignoring the leanocentric principle may lead to wrong conclusions. For example, a more direct and intuitive possibility is that the original adipocytes, by absorbing more nutrients in response to TZDs, can already explain the weight gain. TZDs, through engaging PPAR-γ, upregulate the expression of glucose transporter 4 (GLUT4) on the plasma membrane of adipocytes (Wu et al., 1998). This would give the adipocytes an advantage in competing with the muscles and thus favor the gain of weight. This view may well be wrong for the following reasons. First, the TZDs enhance the body's overall insulin sensitivity; thus, MD must shift to the left (the blue arrow in Figure 7B). That is, myocyte nutrient intake is also enhanced, which compromises adipocyte improvement. Second, even if an adipocyte has managed to grow larger, its nutrient intake capacity immediately decreases due to the increase in its individual insulin resistance (Equation S10), which cancels the effect of the TZDs. Taken together, TZDs are unlikely to promote the growth of the original adipocytes. Indeed, experimental observations have demonstrated the shrinkage but not growth of the existing mature adipocytes (de Souza et al., 2001). In summary, leanocentrism can adequately explain why a likely scenario (the growth of the original adipocytes) cannot actually happen. This, together with the correct prediction of what is actually happening (the generation of new adipocytes), demonstrates the overarching role played by leanocentrism.

Furthermore, we predict that TZD would increase appetite during the early stage of its administration. In the early stage, the newly generated adipocytes are very small and thus very insulin sensitive; they thus absorb large amounts of nutrients, which necessitates large amounts of food intake ("overfeeding"). As the adipocytes grow larger, the "overfeeding" becomes lesser necessary, and the appetite would gradually decrease, approaching the pre-treatment level. This predication can be tested through *ad libitum* feeding of a mouse under continuous TZD treatment. We expect that the mouse develop hyperphagia in the early but not late days of the TZD treatment.

Limitations of the Model

Although the leanocentric locking-point model has considerable explanation and prediction power, its fundamental principles have not yet been firmly established. First, the leanocentric energy balance (Equation 1) depends on the assumption that LM commands energy intake, which, however, has no direct experimental support. Second, the aging-related IR aggravation is critical to explain middle-age spread and is thus the key to demonstrate the merits of the present theory over the lipostatic theory. Although having some supportive data, the assumption needs further testing by more rigorous experiments.

The ODE model was designed to simulate a sedentary adult's FM change during aging. It has to be modified before being used in the other circumstances. To simulate the athletes' body energy metabolism, for example, at least some parameter values need to be changed because the canonical parameter values used by the model were estimated from data on sedentary people. Our theory can explain TZD-induced adipose tissue remodeling, but the validation of the explanation necessitates an extension of the ODE model by at least including new adipocyte recruitment. The extended model can then be used to validate our explanation by fitting its simulation runs with some TZD experimental or clinical data.

Leanocentrism is valid under most conditions but may become irrelevant under some extreme conditions, such as the leptin deficiency in ob/ob mice, which causes them to constantly overeat. The mice rapidly develop obesity. As their adipocytes become increasingly large, the AD consistently moves toward the right with no regard to the position of the MD. On the other hand, the ever-increasing muscle fat deposition continuously exacerbates insulin resistance and drives the MD toward the right. Because now AD commands the movement of MD, it is clearly a case of adipocentrism instead of leanocentrism. Therefore, leanocentrism is not a tenet, although it is applicable to most circumstances.

Resource Availability

Lead Contact

Further information and requests for resources should be directed to and will be fulfilled by the Lead Contact, Guanyu Wang (wanggy@sustech.edu.cn).

Materials Availability

This study did not generate new unique reagents.

Data and Code Availability

Data and code are freely available (Mendeley Data: http://dx.doi.org/10.17632/ts2dzkpz8v.2 or https://data.mendeley.com/datasets/ts2dzkpz8v/draft?a=8dd058ef-8d0c-42fa-8b59-cd99e0e5a9e2).

METHODS

All methods can be found in the accompanying Transparent Methods supplemental file.

SUPPLEMENTAL INFORMATION

Supplemental Information can be found online at https://doi.org/10.1016/j.isci.2020.101176.

ACKNOWLEDGMENTS

This work was partly supported by National Natural Science Foundation of China (61773196), Guangdong Research Funds (2017B030301018, 2019B030301001, 2020KZDZX1182), Shenzhen Research Funds (ZDSYS20140509142721429, JCYJ20170817104740861), Shenzhen Peacock Plan (KQTD2016053117035204), and by Center for Computational Science and Engineering of Southern University of Science and Technology.

AUTHOR CONTRIBUTIONS

G.W. conceived and designed the study, performed the research, analyzed the data, and wrote the paper.

DECLARATION OF INTERESTS

The author declares no competing interests.

Received: January 19, 2020
Revised: April 5, 2020
Accepted: May 14, 2020
Published: June 26, 2020

REFERENCES

Ashwell, M., Meade, C., Medawar, P.B., and Sowter, C. (1977). Adipose tissue: contributions of nature and nurture to the obesity of an obese mutant mouse (ob/ob). Proc. R. Soc. Lond. B *195*, 343–353.

Bedinger, D.H., Goldfine, I.D., Corbin, J.A., Roell, M.K., and Adams, S.H. (2015). Differential pathway coupling of the activated insulin receptor drives signaling selectivity by XMetA, an allosteric partial agonist antibody. J. Pharmacol. Exp. Ther. *353*, 35–43.

Blundell, J., Finlayson, G., Gibbons, C., Caudwell, P., and Hopkins, M. (2015). The biology of appetite control: do resting metabolic rate and fat-free mass drive energy intake? Physiol. Behav. *152*, 473–478.

Bonadonna, R.C., Leif, G., Kraemer, N., Ferrannini, E., Del Prato, S., and DeFronzo, R.A. (1990). Obesity and insulin resistance in humans: a dose-response study. Metabolism *39*, 452–459.

Bonadonna, R.C., Saccomani, M.P., Cobelli, C., and DeFronzo, R.A. (1993). Effect of insulin on system A amino acid transport in human skeletal muscle. J. Clin. Invest. *91*, 514–521.

Chow, C.C., and Hall, K.D. (2014). Short and long-term energy intake patterns and their implications for human body weight regulation. Phys. Behav. *134*, 60–65.

Cieniewicz, A.M., Kirchner, T., Hinke, S.A., Nanjunda, R., DAquino, K., Boayke, K., Cooper, P.R., Perkinson, R., Chiu, M.L., Jarantow, S., et al. (2017). Novel monoclonal antibody is an allosteric insulin receptor antagonist that induces insulin resistance. Diabetes *66*, 206–217.

Creasy, S.A., Rynders, C.A., Bergouignan, A., Kealey, E.H., and Bessesen, D.H. (2018). Free-living responses in energy balance to short-term overfeeding in adults differing in propensity for obesity. Obesity *26*, 696–702.

Cruz-Jentoft, A.J., and Sayer, A.A. (2019). Sarcopenia. Lancet *393*, 2636–2646.

de Souza, C.J., Eckhardt, M., Gagen, K., Dong, M., Chen, W., Laurent, D., and Burkey, B.F. (2001). Effects of pioglitazone on adipose tissue remodeling within the setting of obesity and insulin resistance. Diabetes *50*, 1863–1871.

Dulloo, A.G. (2017). Collateral fattening: when a deficit in lean body mass drives overeating. Obesity *25*, 277–279.

Dulloo, A.G., Jacquet, J., Miles-Chan, J.L., and Schutz, Y. (2017). Passive and active roles of fat-free mass in the control of energy intake and body composition regulation. Eur. J. Clin. Nutr. *71*, 353.

Dybala, M.P., Brady, M.J., and Hara, M. (2019). Disparity in adiposity among adults with normal body mass index and waist-to-height ratio. iScience *21*, 612–623.

Edholm, O., Fletcher, J., Widdowson, E.M., and McCance, R. (1955). The energy expenditure and food intake of individual men. Br. J. Nutr. *9*, 286–300.

Engfeldt, P., and Arner, P. (1987). Lipolysis in human adipocytes, effects of cell size, age and of regional differences. Horm. Metab. Res. Suppl. *19*, 26–29.

Evans-Molina, C. (2011). Understanding PPAR-γ action—just use your brain! Sci. Transl. Med. *3*, 84ec77.

Ferrucci, L., De Cabo, R., Knuth, N.D., and Studenski, S. (2012). Of Greek heroes, wiggling worms, mighty mice, and old body builders. J. Gerontol. A Biol. Sci. Med. Sci. *67A*, 13–16.

Fink, R.I., Kolterman, O.G., Griffin, J., and Olefsky, J.M. (1983). Mechanisms of insulin resistance in aging. J. Clin. Invest. *71*, 1523–1535.

Forbes, G.B. (2000). Body fat content influences the body composition response to nutrition and exercise. Ann. N Y Acad. Sci. *904*, 359–365.

Forbes, G.B. (2012). Human Body Composition: Growth, Aging, Nutrition, and Activity (Springer Science & Business Media).

Frederich, R.C., Hamann, A., Anderson, S., Löllmann, B., Lowell, B.B., and Flier, J.S. (1995). Leptin levels reflect body lipid content in mice: evidence for diet-induced resistance to leptin action. Nat. Med. *1*, 1311–1314.

Goldbeter, A., and Wolpert, L. (1990). Covalent modification of proteins as a threshold mechanism in development. J. Theor. Biol. *142*, 243–250.

Guilherme, A., Virbasius, J.V., Puri, V., and Czech, M.P. (2008). Adipocyte dysfunctions linking obesity to insulin resistance and type 2 diabetes. Nat. Rev. Mol. Cell. Biol. *9*, 367–377.

Havel, R.J., Naimark, A., and Borchgrevink, C.F. (1963). Turnover rate and oxidation of free fatty acids of blood plasma in man during exercise: studies during continuous infusion of palmitate-1-C14. J. Clin. Invest. *42*, 1054.

Herman, C.P., and Polivy, J. (1983). A boundary model for the regulation of eating. Psychiat. Ann. *13*, 918–927.

Kahn, C.R. (1994). Insulin action, diabetogenes, and the cause of type II diabetes. Diabetes *43*, 1066–1085.

Kennedy, G.C. (1953). The role of depot fat in the hypothalamic control of food intake in the rat. Proc. R. Soc. Lond. B *140*, 578–592.

Kim, G., Lee, Y., Yun, M., Lee, J., Shin, E., Lee, B., Kang, E., and Cha, B. (2018a). Effects of lobeglitazone, a novel thiazolidinedione, on adipose tissue remodeling and brown and beige adipose tissue development in db/db mice. Int. J. Obes. *42*, 542–551.

Kim, Y.-J., Greimel, P., and Hirabayashi, Y. (2018b). GPRC5B-mediated sphingomyelin synthase 2 phosphorylation plays a critical role in insulin resistance. iScience *8*, 250–266.

Kita, M., Nakae, J., Kawano, Y., Asahara, H., Takemori, H., Okado, H., and Itoh, H. (2019). Zfp238 regulates the thermogenic program in cooperation with Foxo1. iScience *12*, 87–101.

Leibel, R. (2008). Molecular physiology of weight regulation in mice and humans. Int. J. Obes. *32*, S98–S108.

Leibel, R.L., and Hirsch, J. (1984). Diminished energy requirements in reduced-obese patients. Metabolism *33*, 164–170.

Leibel, R.L., Rosenbaum, M., and Hirsch, J. (1995). Changes in energy expenditure resulting from altered body weight. N. Engl. J. Med. *332*, 621–628.

Li, T., and Wang, G. (2014). Computer-aided targeting of the PI3K/Akt/mTOR pathway: toxicity reduction and therapeutic opportunities. Int. J. Mol. Sci. *15*, 18856–18891.

Lissner, L., Habicht, J.-P., Strupp, B.J., Levitsky, D., Haas, J.D., and Roe, D. (1989). Body composition and energy intake: do overweight women overeat and underreport? Am. J. Clin. Nutr. *49*, 320–325.

MacLean, P.S., Blundell, J.E., Mennella, J.A., and Batterham, R.L. (2017). Biological control of appetite: a daunting complexity. Obesity *25*, S8–S16.

Metter, E.J., Lynch, N., Conwit, R., Lindle, R., Tobin, J., and Hurley, B. (1999). Muscle quality and age: cross-sectional and longitudinal comparisons. J. Gerontol. A Biol. Sci. Med. Sci. *54*, B207–B218.

Mitchel, J.S., and Keesey, R.E. (1977). Defense of a lowered weight maintenance level by lateral hypothamically lesioned rats: evidence from a restriction-refeeding regimen. Physiol. Behav. *18*, 1121–1125.

Müller, M.J., Geisler, C., Heymsfield, S.B., and Bosy-Westphal, A. (2018). Recent advances in understanding body weight homeostasis in humans. F1000Res. *7*, 1025.

Neel, J.V. (1962). Diabetes mellitus: a "thrifty" genotype rendered detrimental by "progress"? Am. J. Hum. Genet. *14*, 353–362.

Neumann, R.O. (1902). Experimentelle beiträge zur lehre von dem täglichen nahrungsbedarf des menschen unter besonderer berück-sichtigung der notwendigen eiweissmenge. Arc. Hyg. *45*, 1–87.

Passmore, R. (1971). The regulation of body-weight in man. Proc. Nutr. Soc. *30*, 122–127.

Pearson, T., McArdle, A., and Jackson, M. (2015). Nitric oxide availability is increased in contracting skeletal muscle from aged mice, but does not differentially decrease muscle superoxide. Free Radic. Biol. Med. *78*, 82–88.

Perry, R.J., Resch, J.M., Douglass, A.M., Madara, J.C., Kucukdereli, H., Wu, C., Song, J.D., Lowell, B.B., Shulman, G.I., et al. (2019). Leptins hunger-suppressing effects are mediated by the hypothalamic–pituitary–adrenocortical axis in rodents. Proc. Nat. Acad. Sci. U S A *116*, 13670–13679.

Polonsky, K., Given, B., Hirsch, L., Shapiro, E., Tillil, H., Beebe, C., Galloway, J., Frank, B., Karrison, T., and Van Cauter, E. (1988a). Quantitative study of insulin secretion and clearance in normal and obese subjects. J. Clin. Invest. *81*, 435–441.

Polonsky, K., Given, B., and Van Cauter, E. (1988b). Twenty-four-hour profiles and pulsatile patterns of insulin secretion in normal and obese subjects. J. Clin. Invest. *81*, 442.

Quek, L.-E., Krycer, J.R., Ohno, S., Yugi, K., Fazakerley, D.J., Scalzo, R., Elkington, S.D., Dai, Z., Hirayama, A., Ikeda, S., et al. (2020). Dynamic 13C flux analysis captures the reorganisation of adipocyte glucose metabolism in response to insulin. iScience *23*, 100855.

Ravussin, Y., Edwin, E., Gallop, M., Xu, L., Bartolomé, A., Kraakman, M.J., LeDuc, C.A., and Ferrante, A.W., Jr. (2018). Evidence for a non-leptin system that defends against weight gain in overfeeding. Cell Metab. *28*, 289–299.

Ravussin, Y., Leibel, R.L., and Ferrante, A.W. (2014). A missing link in body weight homeostasis: the catabolic signal of the overfed state. Cell Metab. *20*, 565–572.

Ropelle, E.R., Pauli, J.R., Cintra, D.E., Da Silva, A.S., De Souza, C.T., Guadagnini, D., Carvalho, B.M., Caricilli, A.M., Katashima, C.K., Carvalho-Filho, M.A., et al. (2013). Targeted disruption of inducible nitric oxide synthase protects against aging, S-nitrosation, and insulin resistance in muscle of male mice. Diabetes *62*, 466–470.

Rosenbaum, M., and Leibel, R.L. (2016). Models of energy homeostasis in response to maintenance of reduced body weight. Obesity *24*, 1620–1629.

Rothwell, N.J., and Stock, M.J. (1979). Regulation of energy balance in two models of reversible obesity in the rat. J. Comp. Physiol. Psychol. *93*, 1024.

Salans, L.B., Horton, E.S., and Sims, E.A. (1971). Experimental obesity in man: cellular character of the adipose tissue. J. Clin. Invest. *50*, 1005.

Salans, L.B., Knittle, J.L., and Hirsch, J. (1968). The role of adipose cell size and adipose tissue insulin sensitivity in the carbohydrate intolerance of human obesity. J. Clin. Invest. *47*, 153.

Scott, M., and Hwa, T. (2011). Bacterial growth laws and their applications. Curr. Opin. Biotechnol. *22*, 559–565.

Seidell, J.C., and Visscher, T.L. (2000). Body weight and weight change and their health implications for the elderly. Eur. J. Clin. Nutr. *54*, S33.

Sims, E.A., and Horton, E.S. (1968). Endocrine and metabolic adaptation to obesity and starvation. Am. J. Clin. Nutr. *21*, 1455–1470.

Speakman, J.R. (2018a). The evolution of body fatness: trading off disease and predation risk. J. Exp. Biol. *221*, jeb167254.

Speakman, J.R. (2018b). Why lipostatic set point systems are unlikely to evolve. Mol. Metab. *7*, 147–154.

Stecco, C. (2014). Functional Atlas of the Human Fascial System (Elsevier Health Sciences).

Stumvoll, M., Jacob, S., Wahl, H.G., Hauer, B., Loblein, K., Grauer, P., Becker, R., Nielsen, M., Renn, W., and Haring, H. (2000). Suppression of systemic, intramuscular, and subcutaneous adipose tissue lipolysis by insulin in humans. J. Clin. Endocrinol. Metab. *85*, 3740–3745.

Tang, W., Zeve, D., Seo, J., Jo, A.-Y., and Graff, J.M. (2011). Thiazolidinediones regulate adipose lineage dynamics. Cell Metab. *14*, 116–122.

Wang, G. (2010). Singularity analysis of the AKT signaling pathway reveals connections between cancer and metabolic diseases. Phys. Biol. *7*, 046015.

Wang, G. (2012). Optimal homeostasis necessitates bistable control. J. R. Soc. Interface *9*, 2723–2734.

Wang, G. (2014). Raison d'être of insulin resistance: the adjustable threshold hypothesis. J. R. Soc. Interface *11*, 20140892.

West, G.B., Brown, J.H., and Enquist, B.J. (1997). A general model for the origin of allometric scaling laws in biology. Science *276*, 122–126.

West, G.B., Woodruff, W.H., and Brown, J.H. (2002). Allometric scaling of metabolic rate from molecules and mitochondria to cells and mammals. Proc. Nat. Acad. Sci. USA *99*, 2473–2478.

Williamson, D.F. (1993). Descriptive epidemiology of body weight and weight change in US adults. Ann. Intern. Med. *119*, 646.

Wirtshafter, D., and Davis, J.D. (1977). Set points, settling points, and the control of body weight. Phys. Behav. *19*, 75–78.

Wu, Z., Xie, Y., Morrison, R.F., Bucher, N., and Farmer, S.R. (1998). PPARgamma induces the insulin-dependent glucose transporter GLUT4 in the absence of C/EBPalpha during the conversion of 3T3 fibroblasts into adipocytes. J. Clin. Invest. *101*, 22–32.

Yang, J., Eliasson, B., Smith, U., Cushman, S.W., and Sherman, A.S. (2012). The size of large adipose cells is a predictor of insulin resistance in first-degree relatives of type 2 diabetic patients. Obesity *20*, 932–938.

Zeng, W., Lu, Y.-H., Lee, J., and Friedman, J.M. (2015). Reanalysis of parabiosis of obesity mutants in the age of leptin. Proc. Nat. Acad. Sci. USA *112*, E3874–E3882.

Zhang, Y., Proenca, R., Maffei, M., Barone, M., Leopold, L., and Friedman, J.M. (1994). Positional cloning of the mouse obese gene and its human homologue. Nature *372*, 425–432.

iScience, Volume *23*

Supplemental Information

Body Mass Dynamics Is Determined by the Metabolic Ohm's Law and Adipocyte-Autonomous Fat Mass Homeostasis

Guanyu Wang

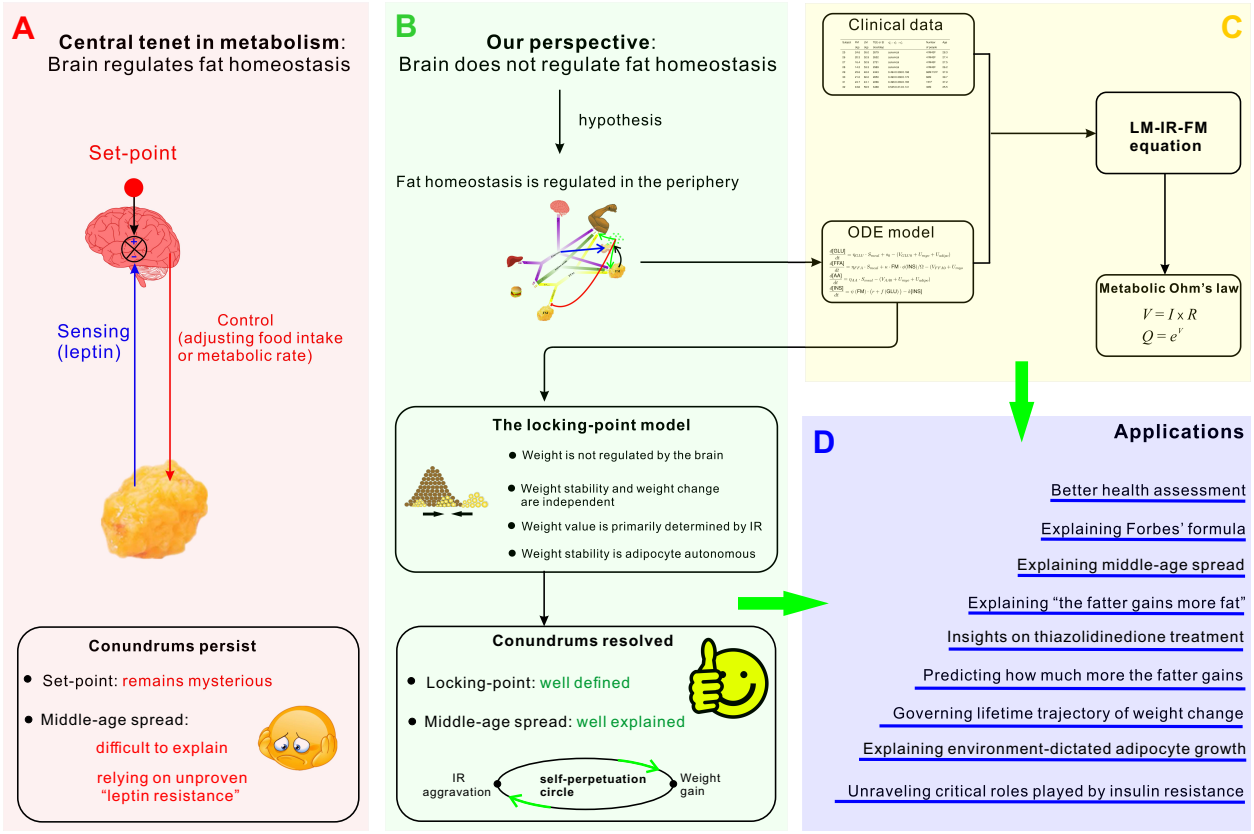

Figure S1: **Road map of the present paper**. Related to Figures 1 and 2. (A) The consensus view is that body weight is regulated by the brain through leptin signaling, although major conundrums remain unresolved. (B) We believe that body weight is not regulated by the brain. Through ordinary differential equation (ODE) modeling of peripheral dynamics, we formulated a leanocentric locking-point model, which resolves all the major conundrums, especially middle-age spread. (C) The integration of the ODE model with clinical data leads to a coarse-grained model, namely, the LM-IR-FM equation, which further leads to the metabolic Ohm's law. (D) The metabolic Ohm's law has a variety of applications.

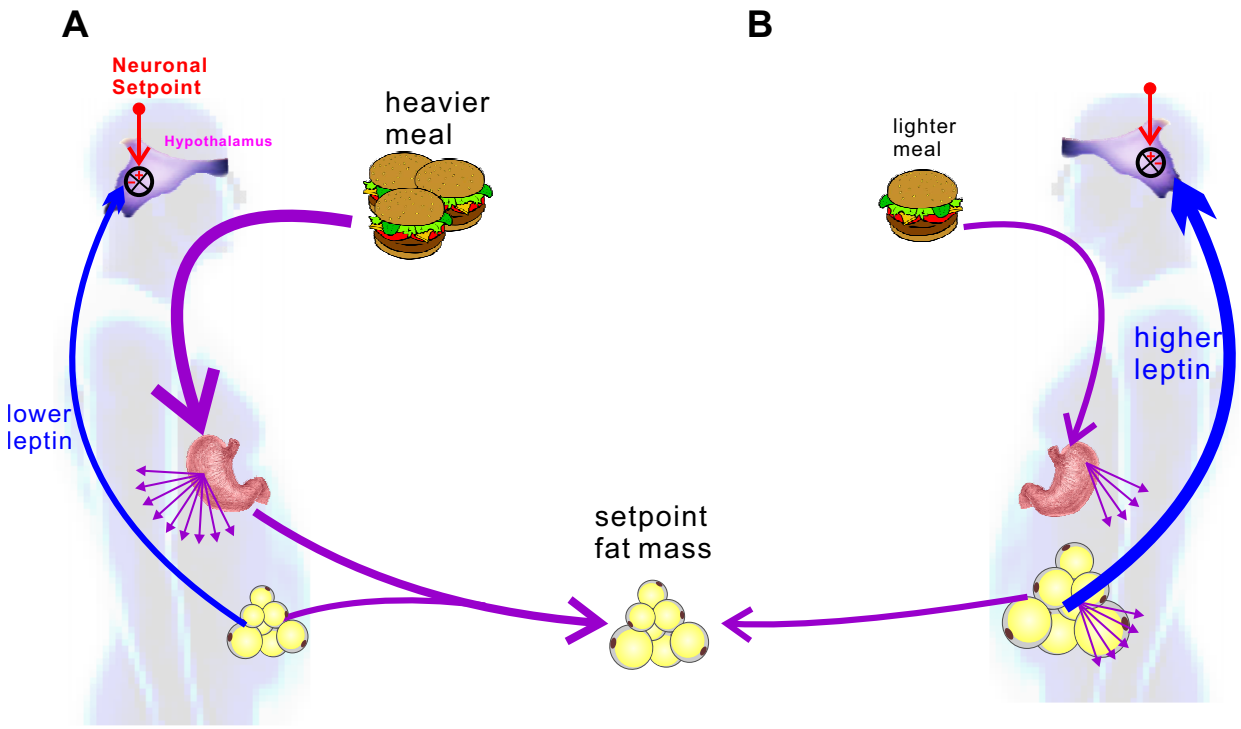

Figure S2: **The lipostatic theory of fat mass homeostasis**. Related to Figure 2. It is believed that our body weight is under active regulation by the CNS, which is well informed of the body's fat level because it can sense the concentration of leptin, a hormone secreted by adipose tissues. (A) When the fat mass is far below the set-point value, the leptin level is reduced, and the brain responds by increasing appetite and decreasing metabolism, trying to increase weight. The acquired nutrients are more than the body actually needs, and the fat mass increases towards the set-point value. (B) When the fat mass becomes far above the set-point value, the circulating leptin level increases, and the brain responds by decreasing appetite and increasing metabolism. Since the acquired nutrients are insufficient, the stored fat is utilized for metabolism, and its mass decreases towards the set-point value.

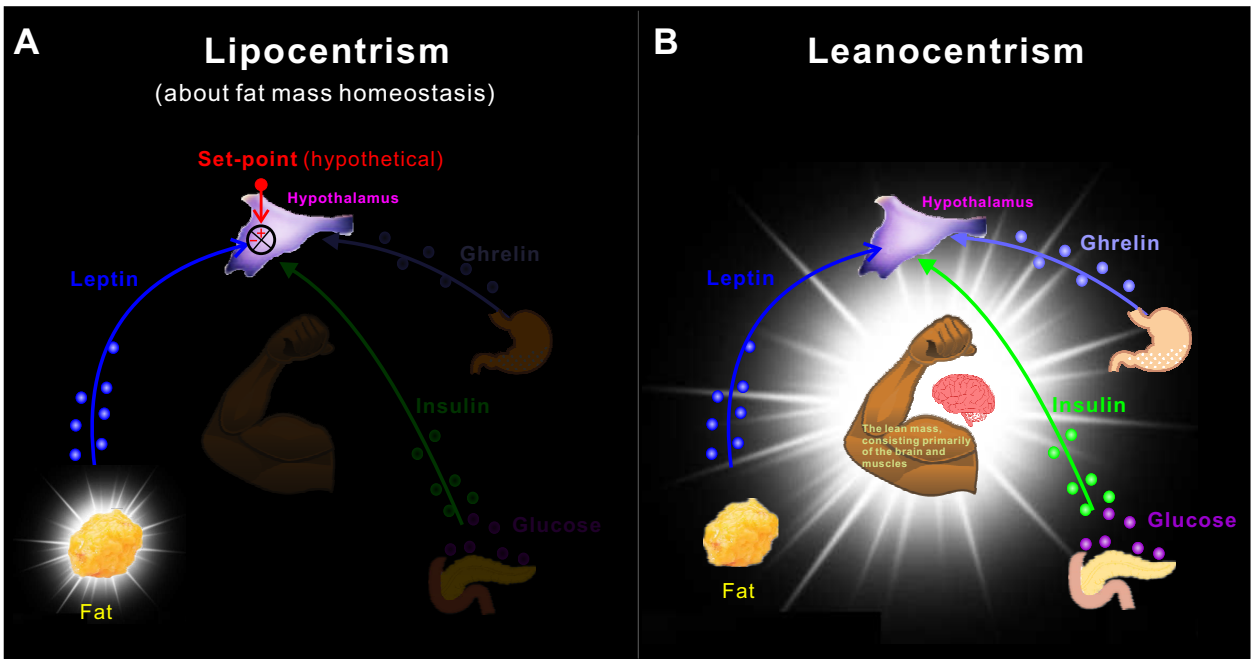

Figure S3: **Paradigm shift from lipocentrism to leanocentrism**. Related to Figures 1 and 2. (**A**) In the lipostatic theory, body fat is the target of regulation, with the leptin concentration as the signal to be compared to a hypothetical set-point in the hypothalamus. (**B**) In the leanocentric paradigm, the lean body mass is the target of energy surveillance. Fat is only one of several energy substrates utilized by the lean tissues and monitored by the CNS.

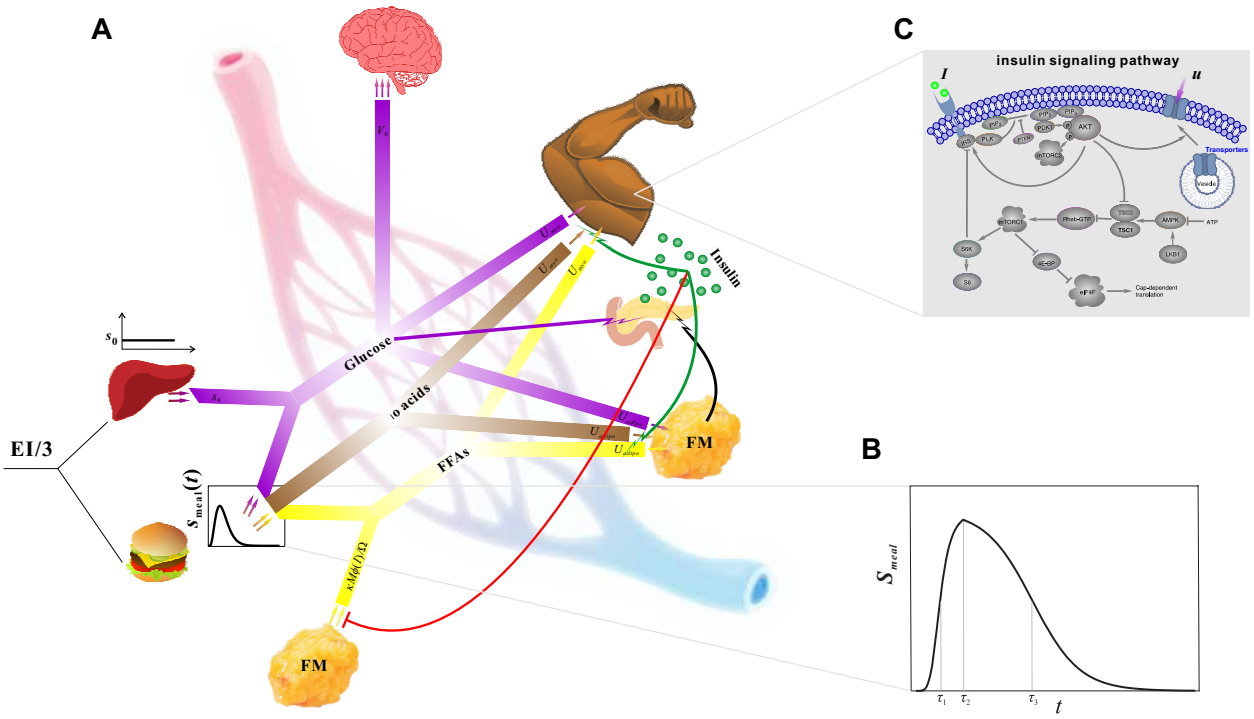

Figure S4: **Peripheral dynamics**. Related to Figures 2, 3, and 4. (A) Dynamical interplay among peripheral tissues, plasma insulin, and plasma nutrients. Plasma glucose (purple) is from either the liver or the meal and is distributed primarily among the brain, muscles, and adipose tissues. The glucose distribution of the latter two depends heavily on the plasma insulin (the green dots), which is secreted by the pancreas upon glucose stimulation (the purple lightning-headed arrow). The insulin secretion becomes greater as the body fat increases (the black lightning-headed arrow). Amino acids (brown) are from the meal. FFAs (yellow) are from either adipose tissues or the meal. They are distributed to muscles and adipose tissues, again depending on insulin. On the other hand, insulin inhibits lipolysis (the red bar-headed arrow). (B) The meal supply function $S_{meal}(t)$ (see Eq. S13). It is the source rate of nutrients as a function of time. (C) Insulin signaling pathway. Upon binding to its receptor, insulin triggers a chain of molecular interactions inside the cell. The signal propagates through the cytoplasm and eventually causes the activation of Akt and the subsequent translocation of nutrient transporters to the plasma membrane, whereby nutrients can be massively transported into the cell.

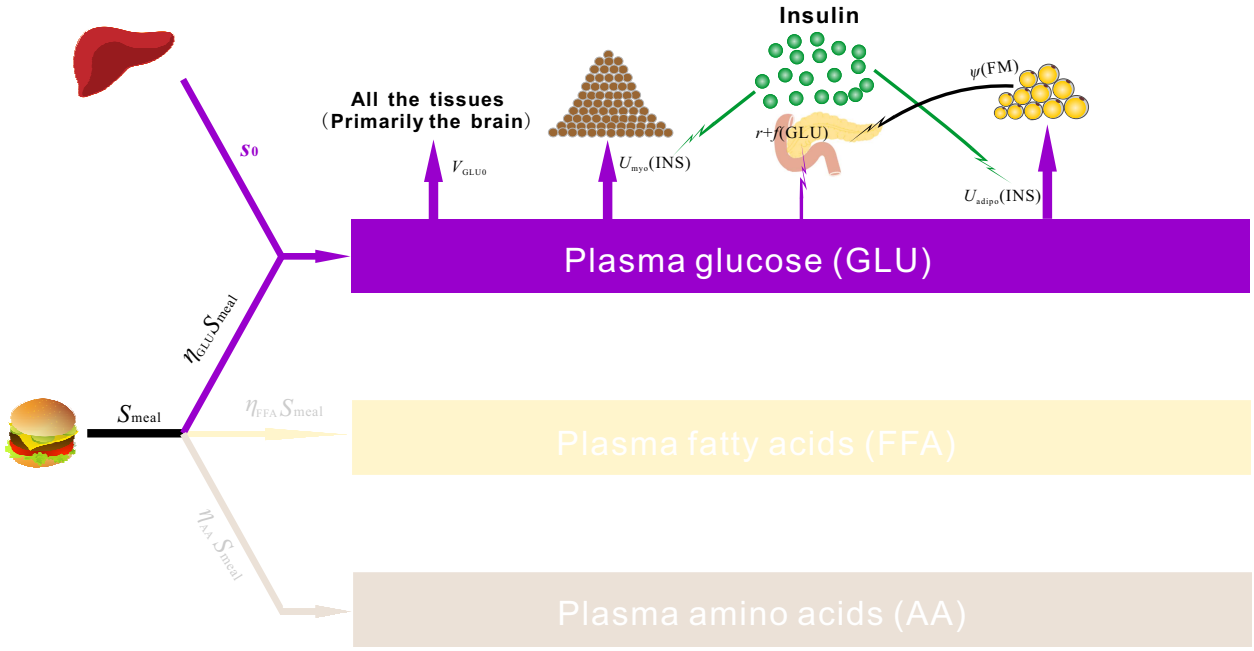

Figure S5: **Plasma glucose-insulin dynamics**. Related to Figures 2, 3, and 4.

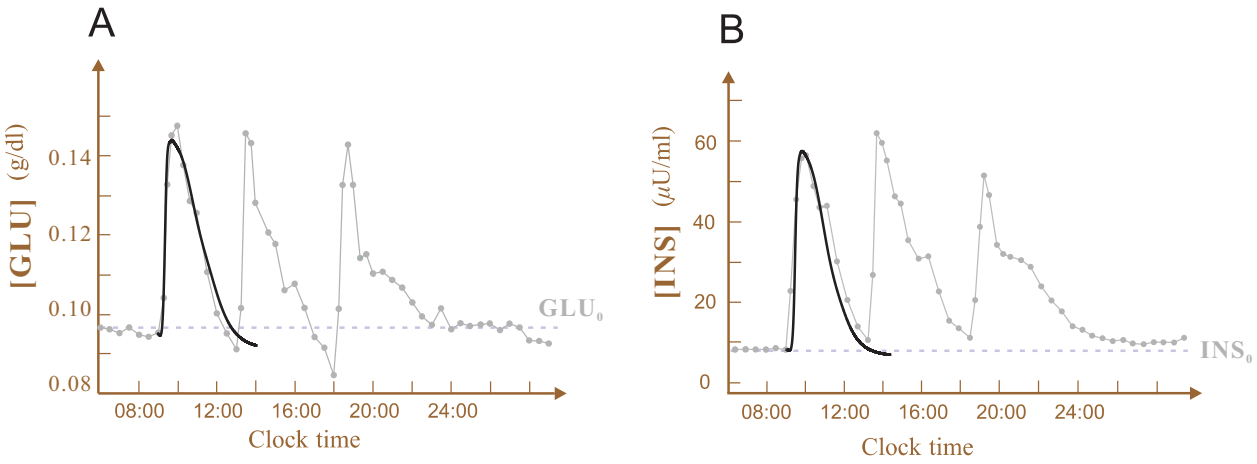

Figure S6: **Plasma glucose dynamics (A) and insulin dynamics (B)**. Related to Figures 2, 3, and 4. The gray dots connected by gray lines represent normal subjects' clinical glucose and insulin concentration profiles, with the three meals beginning at 09:00, 13:00 and 18:00 (Polonsky et al., 1988b). The black curves represent the glucose and insulin dynamics simulated by the ODE model with the canonical parameter values.

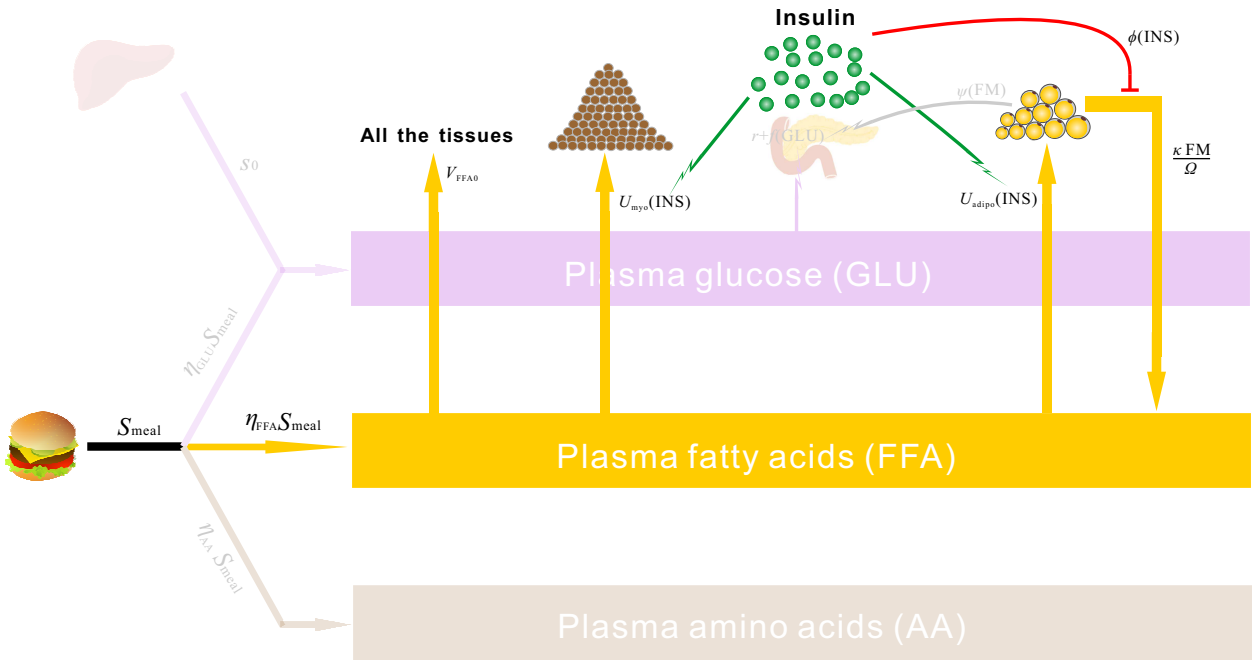

Figure S7: **Plasma FFA dynamics**. Related to Figures 2, 3, and 4.

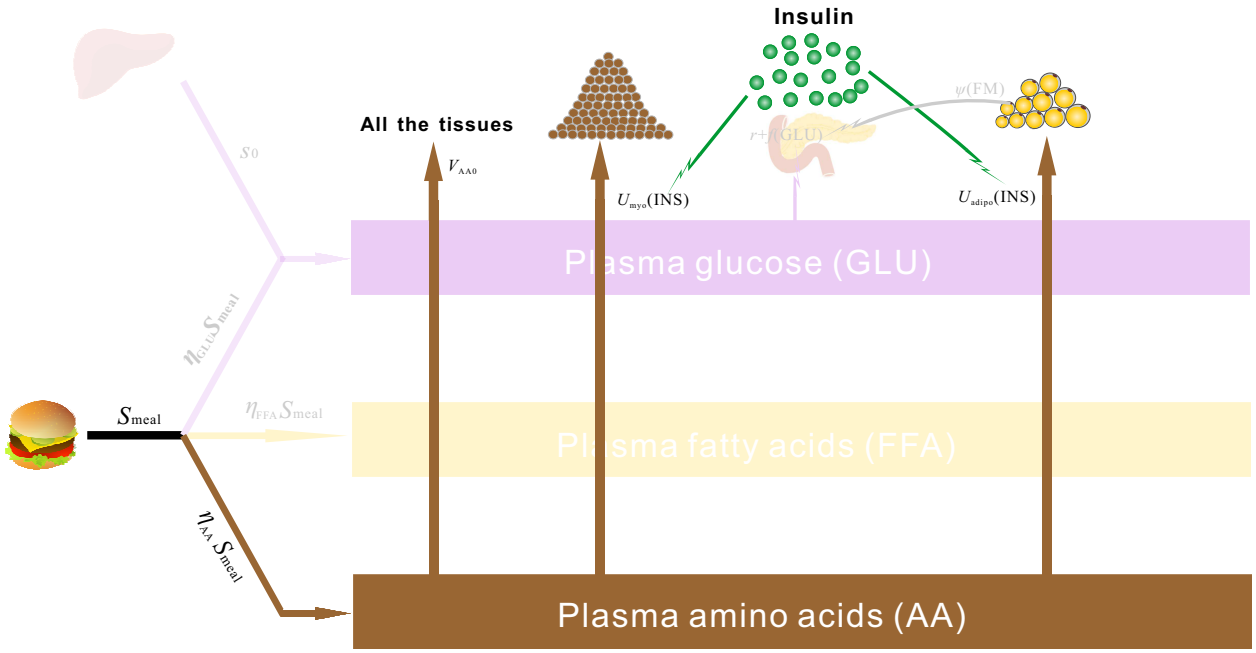

Figure S8: **Plasma AA dynamics**. Related to Figures 2, 3, and 4.

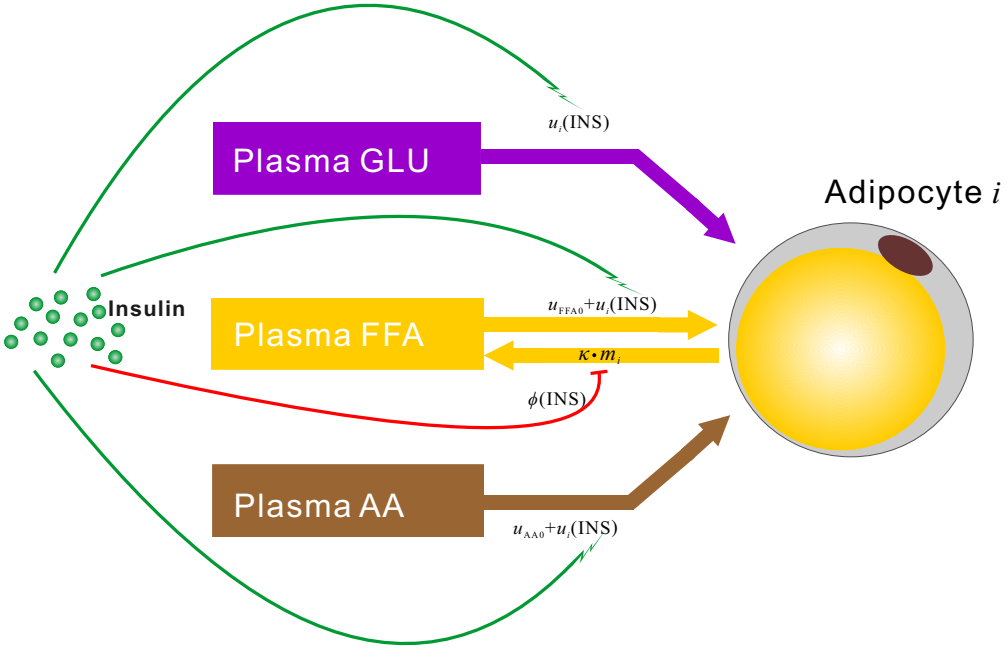

Figure S9: **Dynamics of adipocyte growth**. Related to Figures 2, 3, and 4.

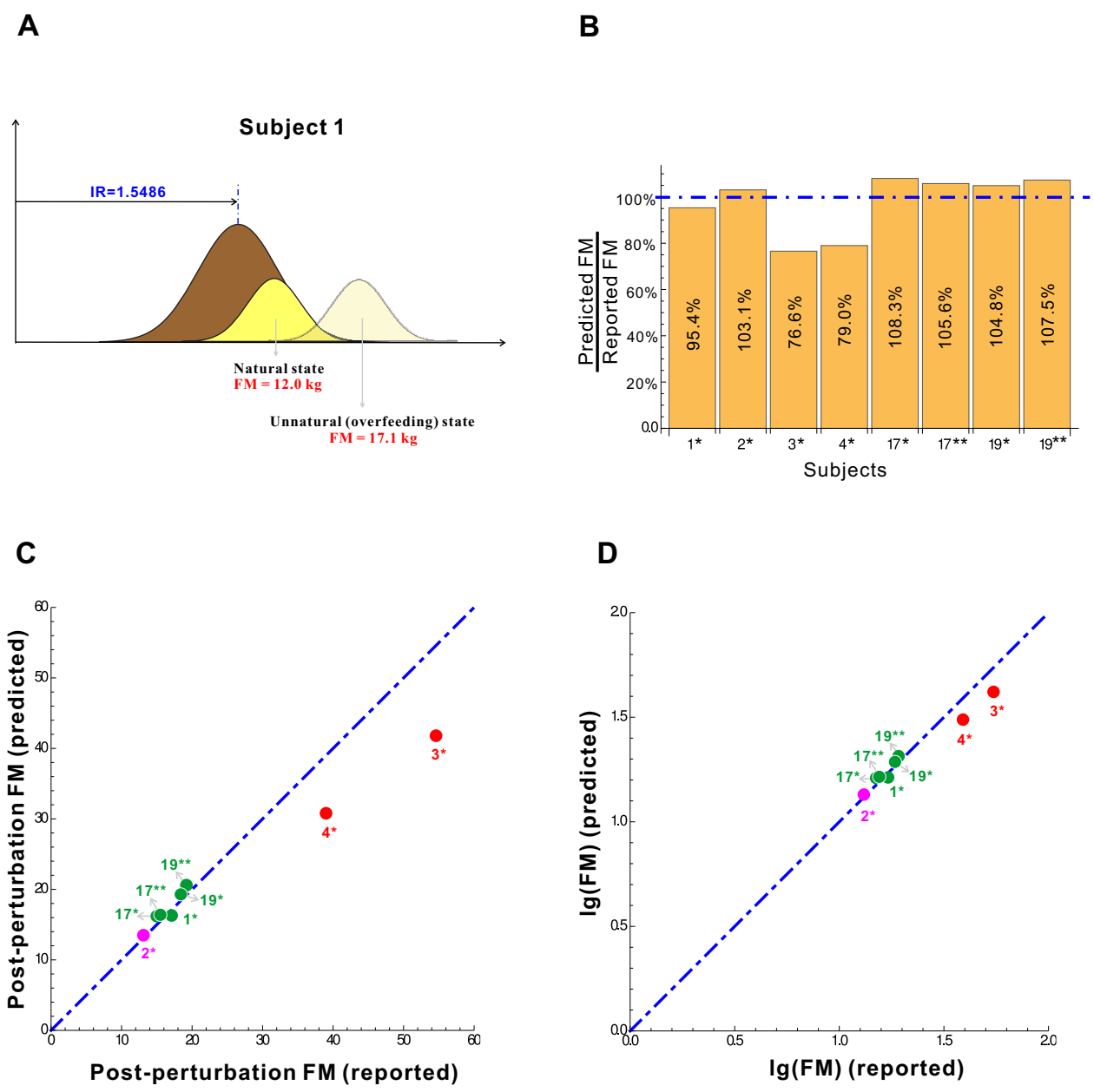

Figure S10: **Testing the ODE model accuracy in predicting the new body fat mass upon overfeeding or underfeeding**. Related to Figures 2 and 3. In total eight perturbations were tested. All the blue lines indicate 100 % accuracy. (A) Subject 1's natural and unnatural states. (B) The ratio of the predicted FM to the reported FM. (C) The reported (predicted) FM of the subjects are presented as the horizontal (vertical) coordinate of the corresponding dots. (D) The reported (predicted) lg(FM) values of the subjects are presented as the horizontal (vertical) coordinates of the corresponding dots.

Table S1: Canonical parameter values. Related to Figures 2, 3, and 4.

Parameter	Value	Unit	Remark
T	480.0	min	The meal cycle. By apportioning one day to the three meal cycles, one obtains T = 8 hour = 480 min.
FFA_0	1.25×10^{-4}	$\mathrm{kg}\times\mathrm{L}^{-1}$	The fasting FFA level. Taken from (Havel et al., 1963).
GLU_0	9.50×10^{-4}	$\mathrm{kg}\times\mathrm{L}^{-1}$	The fasting glucose level. Taken from (Polonsky et al., 1988b).
INS_0	8.00	$\mu\mathrm{U}\times\mathrm{mL}^{-1}$	The fasting insulin level. Taken from (Polonsky et al., 1988b).
σ_{myo}	0.35	$lg(\mu\mathrm{U}\times\mathrm{mL}^{-1})$	The standard deviation of the normal distribution of the myocytes' lg(INS_{on}) values. It usually pairs with IR to represent the normal distribution, namely (IR, σ_{myo}). The value 0.35 was taken from (Wang, 2014).
V_{GLU0}	0.0207	min^{-1}	Estimated from Figure 1 of (Bonadonna et al., 1990).
V_{max}	0.139	min^{-1}	Estimated from Figure 1 of (Bonadonna et al., 1990).
u_{max}	1.183×10^{-5}	min^{-1}	It equals $(V_{max} - V_{GLU0}) / (N_{adipo} + N_{myo})$.
$\mu_{u_{max}}$	1.183×10^{-5}	min^{-1}	The mean of u_{max} when it is randomized.
$\sigma_{u_{max}}$	6.00×10^{-6}	min^{-1}	The standard deviation of u_{max} when it is randomized.
V_{FFA0}	0.200	min^{-1}	Taken from (Havel et al., 1963).
u_{FFA0}	2×10^{-5}	min^{-1}	It is estimated from $V_{FFA0}/ (N_{adipo} + N_{myo})$.
V_{AA0}	0.118	min^{-1}	Taken from (Bonadonna et al., 1993).
u_{AA0}	1.18×10^{-5}	min^{-1}	It is estimated from $V_{AA0}/ (N_{adipo} + N_{myo})$.
κ	1×10^{-5}	min^{-1}	Estimated in .
Ω	5.0	L	An adult's blood volume is about 5 liters (Lee, 1998).
$\rho_{GLU}, \rho_{FFA}, \rho_{AA}$	$4200, 9400, 4700$	$\mathrm{kcal}\times\mathrm{kg}^{-1}$	Energy densities of glucose, fat, and protein (Hall, 2006).
$\eta'_{GLU} : \eta'_{FFA} : \eta'_{AA}$	$0.500 : 0.300 : 0.200$	dimensionless	Calorie percentage of glucose, fat, and protein in the food.
$\eta_{GLU} : \eta_{FFA} : \eta_{AA}$	$0.615 : 0.165 : 0.220$	dimensionless	Mass percentage of glucose, fat, and protein in the food, which can be converted from calorie percentage by $\eta_i = \eta'_i/\rho_i/(\eta'_{GLU}/\rho_{GLU} + \eta'_{FFA}/\rho_{FFA} + \eta'_{AA}/\rho_{AA})$, for $i = GLU, FFA, AA$.
s_0	2×10^{-5}	$\mathrm{kg}\times\mathrm{L}^{-1}\times\mathrm{min}^{-1}$	Steady state condition $s_0 = V_{GLU0}G_0 = 2 \times 10^{-5}$
k	0.322	min^{-1}	Taken from (Wang, 2014), with adjustment.
$f_{\max}$	35.52	$\mu\mathrm{U}\times\mathrm{mL}^{-1}\mathrm{min}^{-1}$	Taken from (Wang, 2014), with adjustment.
GLU_h	1.443×10^{-3}	$\mathrm{kg}\times\mathrm{dL}^{-1}$	Taken from (Wang, 2014), with adjustment.
n	6.432	dimensionless	Taken from (Wang, 2012; Wang, 2014), with adjustment.
r	0.285	$\mu\mathrm{U}\times\mathrm{mL}^{-1}\mathrm{min}^{-1}$	Steady state condition $r = k\mathrm{INS}_0 - f(\mathrm{GLU}_0) = 0.285$
τ_1	19.03	min	Taken from (Wang, 2012; Wang, 2014), with adjustment.
τ_2	40.20	min	Taken from (Wang, 2012; Wang, 2014), with adjustment.
τ_3	103.2	min	Taken from (Wang, 2012; Wang, 2014), with adjustment.
b	4.064	dimensionless	Taken from (Wang, 2012; Wang, 2014), with adjustment.
c	0.0482	min^{-1}	Taken from (Wang, 2012; Wang, 2014), with adjustment.
ψ_0	0.4265	dimensionless	Estimated in .
ψ_1	3.443×10^{-2}	kg^{-1}	Estimated in .
N_{myo}	8000	dimensionless	The number of in silico myocytes.
N_{adipo}	2000	dimensionless	The number of in silico adipocytes.
α	-4.000	dimensionless	Standard value used in (Wang, 2010).
K	0.050	dimensionless	Standard value used in (Wang, 2010).
INS_h	7.3	$\mu\mathrm{U}\times\mathrm{mL}^{-1}$	IC50 of insulin inhibiting lipolysis. Taken from (Stumvoll et al., 2000).
n_0	2.0	dimensionless	The Hill coefficient of insulin inhibiting lipolysis. It was arbitrarily chosen.
ξ	1.5×10^{-4}	$\mathrm{kg}\times\mathrm{mL}\times(\mu\mathrm{U})^{-1}$	Suppose the fat mass is 20 kg and because there are 2000 *in silico* adipocytes, the average mass of an adipocyte is at the order of 10^{-2} kg. If the adipocyte's lg(INS_{on}) value is 2, then one finds ξ is at the order of $10^{-2}/10^2 = 10^{-4}$.

Table S2: Fat mass at different IR, TEE/EI, $\sigma_{u_{\max}}$, N_{adipo} values. Related to Figures 2, 3, and 4. Subjects A1–A4 correspond to Figure 3(A1–A4). Subjects 1, 2, 3, 4, 13, 17, 19 correspond to those in Table S3. Subjects 1*, 2*, 3*, 4*, 17*, 19*, 17**, 19** correspond to those in Table S4.

Subject	IR lg(μU$\times$mL^{-1})	TEE/EI (kcal$\times$day^{-1})	$\sigma_{u_{max}}$ (min^{-1})	N_{adipo}	FM (kg)	FM (kg) (reported)
A1	1.8000	2400	0	2000	18.7	
A2	2.0000	2400	0	2000	27.9	
A3	1.8000	2400	6×10^{-6}	2000	17.9	
A4	2.0000	2400	6×10^{-6}	2000	26.2	
1	1.5486	2481	6×10^{-6}	2000	12.0	12.0
1*	1.5486	3110	6×10^{-6}	2000	16.3	17.1
2	1.8365	2380	6×10^{-6}	2000	17.5	17.5
2*	1.8365	1952	6×10^{-6}	2000	13.5	13.1
2 (90% N_{adipo})	1.8365	2380	6×10^{-6}	1800	15.2	
2 (80% N_{adipo})	1.8365	2380	6×10^{-6}	1600	13.0	
3	2.1830	3100	6×10^{-6}	2000	68.0	68.0
3*	2.1830	2549	6×10^{-6}	2000	41.8	54.6
3 (95% N_{adipo})	2.1830	3100	6×10^{-6}	1900	57.3	
3 (90% N_{adipo})	2.1830	3100	6×10^{-6}	1800	48.7	
4	2.1616	3129	6×10^{-6}	2000	64.4	64.4
4*	2.1616	2243	6×10^{-6}	2000	30.8	39.0
13	2.1132	2528	6×10^{-6}	2000	37.7	37.7
13 (95% N_{adipo})	2.1132	2528	6×10^{-6}	1900	33.8	
13 (90% N_{adipo})	2.1132	2528	6×10^{-6}	1800	30.4	
17	1.8480	2556	6×10^{-6}	2000	21.3	21.3
17*	1.8480	2113	6×10^{-6}	2000	16.2	15.0
17**	1.8480	2122	6×10^{-6}	2000	16.4	15.5
19	2.1320	1935	6×10^{-6}	2000	24.4	24.4
19*	2.1320	1666	6×10^{-6}	2000	19.3	18.4
19**	2.1320	1741	6×10^{-6}	2000	20.6	19.2

Table S3: The body composition and metabolic data of 44 subjects. Related to Figures 2, 3, and 4.

Subject	FM (kg)	LM (kg)	TEE or EI (kcal/day)	$\eta'_{GLU} : \eta'_{FFA} : \eta'_{AA}$	Number of people	Age	Remark	Reference
1	12.0	54.5	2481	0.450:0.400:0.150	13	27	Normal	(Leibel et al., 1995)
2	17.5	53.0	2380	0.450:0.400:0.150	11	25	Overweight	(Leibel et al., 1995)
3	68.0	64.1	3100	0.450:0.400:0.150	9	32	Obese	(Leibel et al., 1995)
4	64.4	60.8	3129	0.450:0.400:0.150	10	31	Obese	(Leibel et al., 1995)
5	30.7	48.1	2168	0.550:0.220:0.230	32F	38	Overweight(BMI=29)	(Weinsier et al., 2000)
6	20.4	41.3	2221	0.595:0.210:0.195	27F	31.7	Normal (BMI=23.1)	(Weinsier et al., 2002)
7	16.2	45.6	1945	canonical	16F	31.5	Normal(BMI=22.4)	(Geissler et al., 1987)
8	20.7	54.2	2632	canonical	114M128F	39.7	Overweight(BMI=25.7)	(Hopkins et al., 2019)
9	19.0	65.0	3140	canonical	114M	40.2	Overweight(BMI=26.4)	(Hopkins et al., 2019)
10	21.5	45.2	2179	canonical	128F	39.2	Normal(BMI=24.8)	(Hopkins et al., 2019)
11	17.9	50.5	2325	canonical	21	28.9	Normal(BMI=23.8) but obesity prone	(Creasy et al., 2018)
12	11.7	49.6	2274	canonical	20	27.4	Normal (BMI=20.2) and obesity resistant	(Creasy et al., 2018)
13	37.7	45.2	2528	canonical	29F		Obese(BMI=32.1)	(Hintze et al., 2018)
14	35.3	44.6	2294	canonical	25F		Obese(BMI=31.6)	(Hintze et al., 2018)
15	22.3	54.3	2730	canonical	105M90F	27.9	Overweight(BMI=25.8)	(Shook et al., 2018)
16	20.5	59.3	2382	canonical	22M	37.8	Overweight(BMI=25.6)	(Das et al., 2017)
17	21.3	60.3	2556	canonical	44M	40.5	Overweight(BMI=26.0)	(Das et al., 2017)
18	25.0	43.0	1905	canonical	53F	37.9	Normal (BMI=24.9)	(Das et al., 2017)
19	24.4	43.3	1935	canonical	99F	36.8	Normal(BMI=24.8)	(Das et al., 2017)
20	21.5	54.4	2741	canonical	101M94F	27.8	Overweight(BMI=25.2)	(Drenowatz et al., 2017)
21	10.9	73.1	2826	0.532:0.247:0.221	17M	29.94	Resist-trained athlete	(Moro et al., 2016)
22	11.3	73.9	3007	0.547:0.239:0.214	17M	28.47	Resist-trained athlete	(Moro et al., 2016)
23	31.8	50.4	2708	canonical	13M58F	37.4	Overweight(BMI=29.9)	(Myers et al., 2017)
24	30.9	55.4	2668	canonical	41M44F	28.8	Overweight(BMI=29.6)	(Shook et al., 2015)
25	24.6	55.0	2679	canonical	41M43F	28.3	Overweight(BMI=26.8)	(Shook et al., 2015)
26	20.3	52.9	2652	canonical	41M43F	27.4	Overweight(BMI=25.2)	(Shook et al., 2015)
27	16.4	52.9	2721	canonical	41M43F	27.5	Normal (BMI=23.5)	(Shook et al., 2015)
28	14.2	53.3	2989	canonical	41M43F	26.2	Normal (BMI=23.0)	(Shook et al., 2015)
29	23.6	48.2	2443	0.494:0.338:0.168	66M:151F	37.9	Overweight(BMI=25.2)	(Redman et al., 2013)
30	21.0	60.0	2850	0.490:0.338:0.172	66M	39.7	Overweight(BMI=25.8)	(Redman et al., 2013)
31	24.7	43.1	2266	0.496:0.339:0.165	151F	37.2	Normal (BMI=24.9)	(Redman et al., 2013)
32	9.84	59.5	3468	0.545:0.314:0.141 Converted from the	32M	25.5	Minnesota starvation experiment	(Keys et al., 1950)

Continuation of Table S3

Subject	FM (kg)	LM (kg)	TEE or EI (kcal/day)	$\eta'_{GLU} : \eta'_{FFA} : \eta'_{AA}$	Number of people	Age	Remark	Reference
				reported $\eta_{GLU} : \eta_{FFA} : \eta_{AA}$				
33	12.8	60.4	3603	canonical	54M26F	20.3	Athlete(BMI=22.1)	(Silva et al., 2017b)
34	16.1	49.0	3002	canonical	26F	19.7	Athlete(BMI=21.9)	(Silva et al., 2017b)
35	11.2	65.9	3897	canonical	54M	20.6	Athlete(BMI=22.3)	(Silva et al., 2017b)
36	11.7	59.7	3673	canonical	39M18F	18.7	Athlete(BMI=21.7)	(Silva et al., 2017a)
37	14.3	47.7	3126	canonical	18F	16.8	Athlete(BMI=21.1)	(Silva et al., 2017a)
38	10.6	65.2	3892	canonical	39M	19.6	Athlete(BMI=21.9)	(Silva et al., 2017a)
39	17.5	66.1	3154.8	canonical	13M	30.2	Overweight(BMI=25.6)	(Grund et al., 2001)
40	14.5	77.4	3154.8	canonical	15M	28.2	Resistance trained athlete(BMI=27.4)	(Grund et al., 2001)
41	11.4	62.6	4493.2	canonical	14M	29.6	Endurance trained athlete(BMI=23.2)	(Grund et al., 2001)
42	11.2	62.1	2145	canonical	43M	27.8	Normal (BMI=24.0)	(Schulz et al., 1991)
43	6.6	63.8	2100	canonical	20M	24.5	Endurance trained athlete(BMI=22.1)	(Schulz et al., 1991)
44	13.1	61.2	2458	0.55:0.29:0.16	10M	20	Boxers/Judokas athlete	(Sagayama et al., 2013)

Table S4: Weight perturbation data of subjects 1, 2, 3, 4, 17, 19. Related to Figures 2 and 3.

Subject	FM (kg)	LM (kg)	TEE or EI (kcal/day)	$\eta'_{GLU} : \eta'_{FFA} : \eta'_{AA}$	Number of people	Age	Remark	Reference
1	12.0	54.5	2481	0.450:0.400:0.150	13	27	Normal weight	(Leibel $\mathrm{et\ al.}$, 1995)
1*	17.1	56.0	3110				10% weight gain	
2	17.5	53.0	2380	0.450:0.400:0.150	11	25	Overweight	(Leibel $\mathrm{et\ al.}$, 1995)
2*	13.1	50.6	1952				10% weight loss	
3	68.0	64.1	3100	0.450:0.400:0.150	9	32	Obese	(Leibel $\mathrm{et\ al.}$, 1995)
3*	54.6	59.7	2549				10% weight loss	
4	64.4	60.8	3129	0.450:0.400:0.150	10	31	Obese	(Leibel $\mathrm{et\ al.}$, 1995)
4*	39.0	57.5	2243				20% weight loss	
17	21.3	60.3	2556	canonical	44M	40.5	Overweight(BMI=26.0)	(Das $\mathrm{et\ al.}$, 2017)
17*	15.0	57.3	2113				Calorie Restriction (1 year)	
17**	15.5	57.3	2122				Calorie Restriction (2 year)	
19	24.4	43.3	1935	canonical	99F	36.8	Normal weight(BMI=24.8)	(Das $\mathrm{et\ al.}$, 2017)
19*	18.4	41.6	1666				Calorie Restriction (1 year)	
19**	19.2	41.6	1741				Calorie Restriction (2 year)	

Transparent Methods

The lipostatic set-point theory and its empirical conundrums

The lipostatic theory is incompatible with a number of empirical findings.

- *Set-point ratchet-up* (middle-age spread). Although our weight is quite stable, the set-point value is subject to a bias toward ratcheting up, which leads to a general gain of weight during aging. To resolve the "set-point ratchet-up" conundrum, the concept of *leptin resistance*, a putative pathologic condition under which the brain becomes insensitive to leptin as fat mass increases, was introduced (Frederich et al., 1995; Könner and Brüning, 2012; Myers et al., 2012). Unfortunately, the existence of leptin resistance has not been verified. In contrast, weight perturbation experiments showed no sign of leptin resistance. They demonstrated that weight stability is robust under all the tested conditions, whether the subject is thin and thus leptin sensitive or has higher fat mass and is thus leptin resistant (Sims and Horton, 1968; Leibel et al., 1995). They also demonstrated that both upward and downward deflections of body weight were suppressed equally well (Figure 1F). It is possible that the upward rebound is slightly stronger than the downward rebound, causing the ratchet-up. However, this asymmetric leptin response is only an assumption and quite an *ad hoc* one (Leibel, 2008). Finally, even if leptin resistance exists, its relevance to the set-point ratchet-up phenomenon is questionable. The phenomenon clearly occurred even in historical times when modern obesogenic factors promoting leptin resistance (overnutrition, sedentary lifestyle, etc.) were generally absent. Indeed, the phrase "middle-age spread" has long been used in both the West and East, in both wealthy and poor populations, to describe the widespread occurrence of fat accumulation after entering adulthood. Therefore, set-point ratchet-up should be independent of leptin resistance.

- *Leptin as a fat messenger*. Intervention studies often found that leptin is not as effective as supposed by the lipostatic theory. For example, leptin administration to mice should lead to lethality due to chronic starvation of the mice, but this effect was not observed in response

to the recombinant leptin at any dose or by any mode of delivery (Halaas et al., 1997). This led to the hypothesis that the recombinant leptin lacks a post-translational modification that is present in the native leptin, which was found to be false (Cohen et al., 1996). Researchers then set out to identify leptin-potentiating cofactors and found the protein clusterin**,** but unfortunately, a leptin/clusterin complex is no more potent than leptin alone (Zeng et al., 2015). On the other hand, leptin knockout mice and normal mice should show different patterns of fat regrowth after partial lipectomy**,** but the actual regrowth is quite similar, indicating that leptin is not required for the regulation of total body fat (Harris et al., 2002). These negative data even led some researchers to abandon the idea that leptin is a fat messenger. They tried to establish other entities, such as sensory nerves emanating from white fat, as the fat messenger (Rooks et al., 2004; Pénicaud, 2010).

The other lipocentric models

The two intervention point model

An alternative to the lipostatic set-point is the "two intervention point" model, which concludes from an evolutionary perspective that there exists an optimal fat mass with respect to the trade-off between the risk of starvation and the risk of predation (Herman and Polivy, 1983; Levitsky, 2002; Speakman, 2007). In the model, the optimal weight is no longer a single set-point but a range of weights, e.g., [50 kg, 100 kg], where 50 (100) kg is called the lower (upper) intervention point. When the weight drops below the lower intervention point, the central regulation (with leptin signaling still assumed) activates to reduce the risk of starvation; when the weight exceeds the upper intervention point, the central regulation activates again to reduce the risk of predation (Speakman, 2018a). When the weight falls within the range, it is already optimal and should be indifferent to central regulation, and insensitivity to leptin (i.e., leptin resistance) is thus expected (Speakman, 2018b). Although the model may reduce the urgency to explain leptin resistance, it does not explain the set-point ratchet-up. Indeed**,** if such a nonregulation zone existed, then the body weight would change randomly within the zone without any bias upward or downward (which cannot explain the ratchet-up). Moreover, the nonregulation zone, if it exists, should have already been discovered by weight perturbation experiments. For example, if the weight is perturbed from 70 to 80, then the final weight would be close to 80, without returning to 70, being within the nonregulation zone. Such a discovery has not been reported, to the best of our knowledge. Furthermore, it is necessary to explain the brain's strange response to leptin: sensitive when the weight is smaller than 50 kg, leptin resistant when the weight is between 50 kg and 100 kg, and leptin sensitive again when the weight exceeds 100kg. In conclusion, the two intervention point model has not been proven.

The settling point model

The "settling point model" takes the lean mass into consideration (Wirtshafter and Davis, 1977; Payne and Dugdale, 1977; Speakman et al., 2002; Levitsky, 2005; Horgan, 2011). The underlying

proposition of the model is that when adipose tissue expands, there is also an increase in lean tissue (Svenson $\mathrm{et\ al.}$, 2007). When food intake exceeds energy expenditure, the adipose tissues expand, which leads to an increase in the metabolically active lean tissue and consequently an increase in energy expenditure. At some point, a new steady state will be reached where the increased intake is matched by the elevated expenditure, and at that point, no further increase in adiposity will occur (Speakman $\mathrm{et\ al.}$, 2002; Christiansen $\mathrm{et\ al.}$, 2005; Christiansen $\mathrm{et\ al.}$, 2008). Although the settling point model performs better than the lipostatic set-point model under some conditions, such as perturbation by high-fat diet feeding (Tam $\mathrm{et\ al.}$, 2009), there remain observations that are more easily explained by the lipostatic theory. In particular, the hyperphagia that follows a period of restriction would not be predicted to exist using the settling point model — instead, individuals would be expected to slowly drift back to their original weight when they resumed their original intake and expenditure conditions (Speakman, 2018a).

The ODE computational model

We first present the model equations (the first subsection) and then explain them in detail (the remaining subsections). The readers are suggested to skim over the first subsection and then read more carefully throughout the remaining subsections.

The model equations (divided into four parts)

Part 1. Dynamics of plasma glucose, FFAs, amino acids, and insulin

$$\frac{d\mathsf{GLU}}{dt} = \eta_{GLU} S_{meal} + s_0 - (V_{GLU0} + U_{myo} + U_{adipo})\,\mathsf{GLU} \tag{S1}$$

$$\frac{d\mathsf{FFA}}{dt} = \eta_{FFA} S_{meal} + \kappa \mathsf{FM} \phi(\mathsf{INS})/\Omega - (V_{FFA0} + U_{myo} + U_{adipo})\,\mathsf{FFA} \tag{S2}$$

$$\frac{d\mathsf{AA}}{dt} = \eta_{AA} S_{meal} - (V_{AA0} + U_{myo} + U_{adipo})\,\mathsf{AA} \tag{S3}$$

$$\frac{d\mathsf{INS}}{dt} = \psi\,(\mathsf{FM})\,[r + f\,(\mathsf{GLU})] - k\mathsf{INS} \tag{S4}$$

$$U_{myo} = \sum_{j=1}^{N_{myo}} u_j \tag{S5}$$

$$U_{adipo} = \sum_{i=1}^{N_{adipo}} u_i \tag{S6}$$

$$\mathsf{FM} = \sum_{i=1}^{N_{adipo}} m_i \tag{S7}$$

where

GLU is the plasma glucose concentration.

FFA is the plasma free fatty acid concentration.

AA is the plasma amino acid concentration.

INS is the plasma insulin concentration.

S_{meal} is the source rate of nutrients supplied by the meal; it is further described by Eq. S13.

s_0 is the source rate of glucose supplied by the liver.

η_{GLU}, η_{FFA}, and η_{AA} are the mass percentages of glucose, fat, and protein, respectively, in

the meal.

V_{GLU0} is the basal (non-insulin dependent) rate of glucose intake by the whole body. It is contributed primarily by the brain, which can utilize glucose actively in the absence of insulin.

V_{FFA0} is the basal (non-insulin-dependent) rate of FFA intake.

V_{AA0} is the basal (non-insulin-dependent) rate of intake of amino acids.

U_{myo} is the rate of nutrient intake by the muscles in response to insulin stimulation. It is the sum of the intake by individual myocytes (Eq. S5).

u_j is the rate of insulin-mediated nutrient intake by the j-th myocyte. The function $u_j\,(\mathrm{INS})$ is constrained by Eq. S8.

N_{myo} is the number of *in silico* myocytes.

U_{adipo} is the rate of nutrient intake by the adipose tissue in response to insulin stimulation. It is the sum of the intake by individual adipocytes (Eq. S6).

u_i is the rate of insulin mediated nutrient intake by the i-th adipocyte. The function $u_i\,(\mathrm{INS})$ is constrained by Eq. S8.

N_{adipo} is the number of *in silico* adipocytes.

FM represents the fat mass. It is the sum of the mass from individual adipocytes (Eq. S7).

m_i is the mass of the i-th adipocyte.

κ is the rate of lipolysis.

$\phi\,(\mathrm{INS})$ is a function of insulin inhibiting lipolysis (the red bar-headed arrow in Figure S4); it is further described by Eq. S16.

Ω is the volume of blood in the body.

r is the basal rate of pancreatic insulin secretion.

$f\,(\mathrm{GLU})$ is the rate of pancreatic insulin secretion in response to glucose stimulation (the purple lightning-headed arrow in Figure S4); it is further described by Eq. S14.

$\psi\,(\mathrm{FM})$ is a function of fat mass promoting insulin secretion (the black lightning-headed arrow in Figure S4). It takes into account the fact that both basal and glucose-stimulated insulin secretion increase as body fat increases. It is further described by Eq. S15.

k is the rate of insulin degradation.

Part 2. Insulin response curve u(INS) of an adipocyte or myocyte

Insulin response curve u(INS) is the relationship between the cell rate of insulin-mediated nutrient intake u (the response) and the plasma insulin concentration INS (the stimulus). It is constrained by the following equation

$$0 = \frac{\alpha}{\mathrm{INS}_{on}}\left(\frac{u}{u_{\max}}\right)^3 + \left[(K-1)\frac{\alpha}{\mathrm{INS}_{on}} + \frac{\mathrm{INS}}{\mathrm{INS}_{on}} - 1\right]\left(\frac{u}{u_{\max}}\right)^2 + \left[K+1+(K-1)\frac{\mathrm{INS}}{\mathrm{INS}_{on}} - K\frac{\alpha}{\mathrm{INS}_{on}}\right]\frac{u}{u_{\max}} - K\frac{\mathrm{INS}}{\mathrm{INS}_{on}}, \tag{S8}$$

$$u_{\max} = \left(V_{\max} - V_{GLU0}\right)/(N_{adipo} + N_{myo}),$$

where u and INS are highlighted in red. This equation, obtained by mathematical modeling of the insulin signaling pathway (Wang, 2010; Wang, 2012; Li and Wang, 2014), gives rise to the sigmoidal curves in Figure 2B. Here,

α, INS_{on}, and K are the three parameters determining the shape of u(INS); in particular, INS_{on} is the insulin response threshold (see Figure 2B) and is related to the cell's insulin resistance.

$u_{\max}$ is the cell's maximal rate of insulin mediated nutrient intake (see Figure 2B).

$V_{\max}$ is the maximal rate of glucose intake by the whole body. It can be estimated from the whole-body data (Bonadonna $\mathrm{et\ al.}$, 1990).

V_{GLU0} is the basal (non-insulin-dependent) rate of glucose intake by the whole body.

The above symbols are often followed by a subscript: i to indicate adipocytes and j to indicate myocytes. For example, u_i is the nutrient intake rate of the i-th adipocyte; $(\mathrm{INS}_{on})_j$ is the INS_{on} of the j-th myocyte.

Part 3. Dynamics of adipocyte growth

$$\frac{dm_i}{dt} = \left[u_i\left(\mathsf{GLU}+\mathsf{FFA}+\mathsf{AA}\right)+u_{FFA0}\mathsf{FFA}+u_{AA0}\mathsf{AA}\right]\Omega-\kappa m_i\phi\left(\mathsf{INS}\right) \tag{S9}$$

$$m_i = \xi\left(\mathsf{INS}_{on}\right)_i \tag{S10}$$

where

$u_{FFA0} = V_{FFA0}/\left(N_{myo}+N_{adipo}\right)$ is a cell's basal intake rate of FFAs.

$u_{AA0} = V_{AA0}/\left(N_{myo}+N_{adipo}\right)$ is a cell's basal intake rate of amino acids.

m_i is the mass of the i-th adipocyte.

$\left(\mathsf{INS}_{on}\right)_i$ is the INS_{on} of the i-th adipocyte.

ξ is the scale factor between INS_{on} and m.

Part 4. Leanocentric energy balance

$$\frac{E_{intoLean}}{3} = \frac{\mathsf{TEE}}{3}, \tag{S11}$$

where

$$\frac{E_{intoLean}}{3} = \int_0^T \Big(\rho_{GLU}\cdot V_{GLU0}\cdot\mathsf{GLU}\cdot\Omega+\rho_{GLU}\cdot U_{myo}\cdot\mathsf{GLU}\cdot\Omega+\rho_{FFA}\cdot u_{FFA0}\cdot N_{myo}\cdot\mathsf{FFA}\cdot\Omega$$
$$+\rho_{FFA}\cdot U_{myo}\cdot\mathsf{FFA}\cdot\Omega+\rho_{AA}\cdot u_{AA0}\cdot N_{myo}\cdot\mathsf{AA}\cdot\Omega+\rho_{AA}\cdot U_{myo}\cdot\mathsf{AA}\cdot\Omega\Big)dt. \tag{S12}$$

Equation S11 is apparently equivalent to Eq. 1. Here, the division by 3 is because our computation is on a per meal-cycle basis (see Eq. S.12). The meal cycle, denoted by T, is the period starting with a meal and ending immediately before the next meal. Assuming a day is equally divided by the three meals, we have $T = 8$ hour $= 480$ min. ρ_{GLU}, ρ_{FFA}, and ρ_{AA} are the energy densities of glucose, fat, and protein, respectively.

Dynamics of plasma nutrients and insulin

The meal supply function

The plasma nutrients are primarily from the meal supply, with a rate $S_{meal}(t)$ in the unit of kg$\times$L$^{-1}\times$min^{-1}. The function has a shape with both rising and declining phases (Figure S4B) (Sturis $\mathrm{et\ al.}$, 1991). We used sigmoidal curves to model both the rising phase ($t < \tau_2$) and the declining phase ($t \geq \tau_2$) (Wang, 2012; Wang, 2014)

$$S_{meal}(t) = \begin{cases} A(t/\tau_1)^b / \left[1 + (t/\tau_1)^b\right] & \text{for } 0 \leq t < \tau_2 \\ A\exp\left[c(\tau_3 - t)\right] / \left\{1 + \exp\left[c(\tau_3 - t)\right]\right\} & \text{for } \tau_2 \leq t < \infty \end{cases}, \tag{S13}$$

where the values of b, c, τ_1, τ_2, and τ_3 are given in Table S1. Therefore, the only unknown parameter in $S_{meal}(t)$ is the meal magnitude A. Under the condition of necessary feeding, the food intake EI is determined by the given TEE. In other words, the value of A is usually not given but needs to be calculated according to the given TEE. In food, the mass percentage of glucose, fat, and protein is denoted by η_{GLU}, η_{FFA}, and η_{AA}, which can be converted into the calorie percentages η'_{GLU}, η'_{FFA}, and η'_{AA} by a formula given in Table S1. The calorie percentage is more frequently reported in the literature.

Plasma glucose-insulin dynamics

The plasma glucose-insulin dynamics are described by Figure S5, where the FFA and AA dynamics are blurred so that the glucose-insulin dynamics are highlighted.

Equation S1, namely,

$$\frac{d\mathrm{GLU}}{dt} = \eta_{GLU}S_{meal} + s_0 - (V_{GLU0} + U_{myo} + U_{adipo})\,\mathrm{GLU}$$

describes the dynamics of GLU(t), where $\eta_{GLU}S_{meal}(t)$ is the source rate of glucose from the meal; s_0 corresponds to the hepatic output of glucose. V_{GLU0} is the basal (non-insulin dependent) rate of glucose utilization by the whole body, primarily the brain. $U_{myo} = \sum_j u_j(\mathrm{INS})$ is the total rate of myocyte glucose utilization; it is stimulated by insulin, indicated by the left green lightning-

headed arrow in Figure S5. $U_{adipo} = \sum_i u_i\,(\mathrm{INS})$ is the total rate of adipocytes glucose utilization; it is also stimulated by insulin, indicated by the right green lightning-headed arrow.

Equation S4, namely,

$$\frac{d\mathrm{INS}}{dt} = \psi\,(\mathrm{FM})\,[r + f\,(\mathrm{GLU})] - k\mathrm{INS}$$

describes the dynamics of $\mathrm{INS}(t)$. According to (Bilous and Donnelly, 2010), the pancreatic insulin secretion rate has a basal component r and a glucose-stimulation component $f\,(\mathrm{GLU})$. The latter is indicated by the purple lightning-headed arrow. $f\,(\mathrm{GLU})$ is modeled by a Hill function (Wang, 2012; Wang, 2014)

$$f\,(\mathrm{GLU}) = \frac{f_{\max}}{1 + (\mathrm{GLU}_h/\mathrm{GLU})^n}, \tag{S14}$$

where $f_{\max}$ is the maximum rate of glucose stimulated insulin secretion, GLU_h is the half maximal effective glucose concentration (EC50), and n is the Hill coefficient. Because insulin secretion increases as the fat mass increases (indicated by the black lightning-headed arrow) (Polonsky $\mathrm{et\ al.}$, 1988a), $r + f\,(\mathrm{GLU})$ is multiplied by $\psi(\mathrm{FM})$, an increasing function of fat mass:

$$\psi(\mathrm{FM}) = \psi_0 + \psi_1 \mathrm{FM}. \tag{S15}$$

The parameters ψ_0 and ψ_1 were determined as follows. First, because the model uses the normal subjects in (Polonsky $\mathrm{et\ al.}$, 1988b; Polonsky $\mathrm{et\ al.}$, 1988a) as the reference, we have $\psi(\mathrm{FM}_1) = 1$, where FM_1 is the fat mass of the normal subjects. Second, because the insulin secretion of the obese subjects in (Polonsky $\mathrm{et\ al.}$, 1988b; Polonsky $\mathrm{et\ al.}$, 1988a) was approximately doubled, we have $\psi(\mathrm{FM}_2) = 2$, where FM_2 is the fat mass of the obese subjects. We thus obtain

$$\psi_0 = \frac{\mathrm{FM}_2 - 2\mathrm{FM}_1}{\mathrm{FM}_2 - \mathrm{FM}_1} \text{ and } \psi_1 = \frac{1}{\mathrm{FM}_2 - \mathrm{FM}_1}.$$

The values of FM_1 and FM_2 are not given in (Polonsky $\mathrm{et\ al.}$, 1988b; Polonsky $\mathrm{et\ al.}$, 1988a). We thus estimated the values according to the formula (Deurenberg $\mathrm{et\ al.}$, 1998)

$$\mathrm{FM}\% = 1.294 \times \mathrm{BMI} + 0.2 \times \mathrm{Age} - 11.4 \times \mathrm{Sex} - 8.0.$$

For the normal subjects, $\overline{\text{BMI}} = 23.0$, $\overline{\text{Age}} = 38.5$, and $\overline{\text{Sex}} = 0.5$ (7 male and 7 female); thus, we have $\text{FM}\% = 23.762$ and then $\text{FM}_1 = 70.1 \times 23.762\% = 16.657$ kg. For the obese subjects, $\overline{\text{BMI}} = 37.0$, $\overline{\text{Age}} = 35.8$, and $\overline{\text{Sex}} = 1/3$ (5 male and 10 female); we thus have, $\text{FM}\% = 43.238$ and then $\text{FM}_2 = 105.7 \times 43.238\% = 45.703$ kg. We then obtain $\psi_0 = 0.42653$ and $\psi_1 = 0.0344281$.

The glucose-insulin dynamics were already simulated by an earlier mathematical model (Eqs. 2.1 and 2.2 in (Wang, 2014)). The simulation runs fit well with the clinical data in (Polonsky $\mathrm{et\ al.}$, 1988b; Polonsky $\mathrm{et\ al.}$, 1988a; Bonadonna $\mathrm{et\ al.}$, 1990). In this model, Eq. S1 is based on Eq. 2.1 of (Wang, 2014). The only difference is that $\eta_{GLU} = 1$ in (Wang, 2014) because in that paper FFA and amino acids were not studied. Equation S4 is based on Eq. 2.2 of (Wang, 2014), namely, $d\text{INS}/dt = f(\text{GLU}) - k\text{INS}$. The new parameter r is to take into account the basal (non-glucose-stimulated) insulin secretion (Bilous and Donnelly, 2010). This change necessitated adjustment of the original parameter values so that the new simulation run (the black curves in Figure S6) can still fit well with the clinical data in (Polonsky $\mathrm{et\ al.}$, 1988b; Polonsky $\mathrm{et\ al.}$, 1988a; Bonadonna $\mathrm{et\ al.}$, 1990) (represented by the gray dots in Figure S6).

Plasma FFA dynamics

The plasma FFA dynamics are described by Figure S7, where the GLU and AA dynamics are blurred so that the FFA dynamics are highlighted.

Equation S2, namely,

$$\frac{d\text{FFA}}{dt} = \eta_{FFA} S_{meal} + \kappa \text{FM} \phi(\text{INS})/\Omega - (V_{FFA0} + U_{myo} + U_{adipo})\,\text{FFA}$$

describes the dynamics of $\text{FFA}(t)$, where $\eta_{FFA} S_{meal}\,(t)$ is the source rate of FFA from the meal; $\kappa \text{FM} \phi\,(\text{INS})\,/\Omega$ is the source rate of FFA arising from lipolysis of the FM. Here, Ω is the blood volume, and the division by Ω is for the conversion from the rate of mass change ($\text{kg}\times\text{min}^{-1}$) to the rate of concentration change ($\text{kg}\times\text{L}^{-1}\times\text{min}^{-1}$). A typical adult's blood volume is approxmiately $\Omega = 5.0$ L (Lee, 1998). The function

$$\phi\,(\text{INS}) = \frac{1}{1 + (\text{INS}/\text{INS}_h)^{n_0}} \tag{S16}$$

takes into account the effect of insulin in inhibiting lipolysis (the red bar-headed arrow in Figure S7), where n_0 is the Hill coefficient and INS_h is the half maximal inhibitory insulin concentration (IC50). The value of INS_h was estimated to be approxmiately 51 pM (Stumvoll $\mathrm{et\ al.}$, 2000), that is, $7.3\ \mu$U/mL. The rate of FFA utilization is divided into the basal component V_{FFA0} and the insulin-dependent component $U_{myo} + U_{adipo}$. The experimental value of V_{FFA0} is in the range 0.18 – 0.21 min^{-1} (Havel $\mathrm{et\ al.}$, 1963), and the value $0.20\ \mathrm{min}^{-1}$ was used in this study.

The value of κ was determined by considering the fasting steady-state (when INS = INS_0, FFA = FFA_0, and $U_{myo} = U_{adipo} = 0$):

$$\left.\frac{d\mathrm{FFA}}{dt}\right|_{\mathrm{FFA}=\mathrm{FFA}_0} = \kappa \mathrm{FM}\phi\left(\mathrm{INS}_0\right)/\Omega - V_{FFA0}\mathrm{FFA}_0 = 0,$$

namely,

$$\kappa = \frac{V_{FFA0}\mathrm{FFA}_0\Omega}{\mathrm{FM}\phi\left(\mathrm{INS}_0\right)}.$$

The value of FFA_0 is about 0.0005 mol/L (Havel $\mathrm{et\ al.}$, 1963). It is known that palmitic acid is the main fatty acid in the blood (Abdelmagid $\mathrm{et\ al.}$, 2015). We thus let the molecular weight of an average FFA be that of palmitic acid, namely, 0.25 kg/mol, resulting in $\mathrm{FFA}_0 = 1.25 \times 10^{-4}$ kg/L. By taking FM = 16.657 kg (see above), we obtained $\kappa \approx 10^{-5}\ \mathrm{min}^{-1}$.

Plasma amino acid dynamics

The plasma AA dynamics are described by Figure S8, where the GLU and FFA dynamics are blurred so that the AA dynamics are highlighted.

Equation S3, namely,

$$\frac{d\mathrm{AA}}{dt} = \eta_{AA}S_{meal} - \left(V_{AA0} + U_{myo} + U_{adipo}\right)\mathrm{AA}$$

describes the dynamics of $\mathrm{AA}(t)$, where $\eta_{AA}S_{meal}\left(t\right)$ is the source rate of amino acids from the meal; V_{AA0} is the basal (non-insulin dependent) rate of amino acid utilization by the whole body.

Insulin response curve u(INS) of an adipocyte or myocyte

The fat tissue consists of heterogeneous adipocytes, each responding differentially to insulin. To take heterogeneity into account, N_{adipo} adipocytes are created *in silico*. Each *in silico adipocyte*'s insulin dose response is denoted by $u_i\,(\mathrm{INS})$, where u represents the rate of nutrient intake, and the subscript i numbers the adipocytes. We thus have $U_{adipo} = \sum_{i=1}^{N_{adipo}} u_i$ (Eq. S6). Note that N_{adipo} cannot be too large; otherwise, computational costs would be prohibitive. In this paper, $N_{adipo} = 2000$ is used as the canonical value. If FM = 12 kg, then the mass of an *in silico* adipocyte is on average 0.006 kg, too large for a real adipocyte. Therefore, an *in silico* adipocyte actually corresponds to a collection of many real adipocytes. Similarly, N_{myo} myocytes are created in silico, and their insulin dose responses are denoted by $u_j\,(\mathrm{INS})$. Note that adipocytes and myocytes are distinguished by the subscripts i and j, respectively.

The insulin response curve u(INS) is constrained by an algebraic equation (Eq. S8), namely,

$$0 = \frac{\alpha}{\mathrm{INS}_{on}}\left(\frac{u}{u_{\max}}\right)^3 + \left[(K-1)\frac{\alpha}{\mathrm{INS}_{on}} + \frac{\mathrm{INS}}{\mathrm{INS}_{on}} - 1\right]\left(\frac{u}{u_{\max}}\right)^2 + \left[K+1+(K-1)\frac{\mathrm{INS}}{\mathrm{INS}_{on}} - K\frac{\alpha}{\mathrm{INS}_{on}}\right]\frac{u}{u_{\max}} - K\frac{\mathrm{INS}}{\mathrm{INS}_{on}},$$

$$u_{\max} = \left(V_{\max} - V_{GLU0}\right)/(N_{adipo} + N_{myo}),$$

which was obtained by mathematical modeling of the insulin signaling pathway (Figure S4C) (Wang, 2010; Wang, 2012; Li and Wang, 2014). The equation comprises, in addition to u and INS, four quantities α, K, INS_{on}, and $u_{\max}$. When the values of these four quantities are given, the response curve u(INS) is completely determined. The shape of u(INS) is generally sigmoidal (see, e.g., the curves in Figure 2B).

The symbol INS_{on} shows the intended biological meaning: the turning-on threshold of insulin response. To see this correspondence with ease, one can use the limit condition $K = 0$, whereby Eq. S8 is factored into three linear equations, which correspond to the three straight lines in Figure 2B (drawn in gray). From the geometrical perspective, the intersection of the bottom straight line and the tilted straight line is clearly the insulin response threshold. From the algebraic perspective, some calculation shows that the x-coordinate of the intersection point is precisely INS_{on}.

Therefore, the symbol INS_{on} does have the intended meaning.

The threshold INS_{on} can be used to quantify a cell's insulin resistance. Indeed, the larger the threshold, the more difficult it is for the cell to respond, and the more resistant the cell is to insulin. The increase in INS_{on} leads to an almost parallel shift of the response curve to the right (Wang, 2010; Wang, 2012; Li and Wang, 2014). When $K = 0$, the right-shift is exactly parallel (Figure 2B). This right-shift phenomenon corresponds well to the clinical discovery that exacerbation of insulin resistance can be well characterized by a right-shift in insulin dose response (Olefsky and Kolterman, 1981; Bonadonna et al., 1990; Basu et al., 2004). These features all suggest the suitability of using INS_{on} to quantify a cell's degree of insulin resistance.

In this paper, the $\lg(\text{INS}_{on})$ value, instead of INS_{on}, is used to quantify insulin resistance. This choice is primarily because for a biochemical dose response, it is usually the logarithm of concentration, not the concentration itself, that is plotted on the horizontal axis. This is particularly true for the insulin dose response (Bonadonna et al., 1990; Bedinger et al., 2015; Cieniewicz et al., 2017). Due to cellular heterogeneity, the cells have different degrees of insulin resistance; they spread out over the $\lg(\text{INS}_{on})$-axis and form stable distributions (Figure 2C). Fitting whole-body insulin dose response data reported in (Bonadonna et al., 1990) showed that the body's insulin-responsive cells roughly form a normal distribution over the $\lg(\text{INS}_{on})$-axis (Wang, 2014). The mean of the normal distribution has been denoted by IR in the main text and used to quantify peripheral insulin resistance.

Dynamics of adipocyte growth

The dynamics of adipocyte growth are described by Figure S9.

Equation S9, namely,

$$\frac{dm_i}{dt} = \left[u_i\left(\text{GLU} + \text{FFA} + \text{AA}\right) + u_{FFA0}\text{FFA} + u_{AA0}\text{AA}\right]\Omega - \kappa m_i \phi\left(\text{INS}\right),$$

models the dynamical change in m_i, the mass of the i-th adipocyte. The adipocyte shrinks by default due to the cell's lipolysis $-\kappa m_i$, but the plasma nutrients (GLU, FFA, AA) allow the cell to grow. The rate of nutrient uptake has both basal components $u_{FFA0}\text{FFA}+u_{AA0}\text{AA}$ and insulin-

dependent components $u_i\,(\text{INS})\,(\text{GLU + FFA + AA})$ (the green lightning-headed arrows in Figure S9). The multiplication of the blood volume Ω is for the conversion from the rate of concentration change (kg$\times$L$^{-1}\times$min^{-1}) to the rate of mass change (kg$\times$min^{-1}). Insulin not only promotes adipocyte growth but also inhibits lipolysis through the function $\phi\,(\text{INS})$ (the red bar-headed arrow in Figure S9). Note that the dynamics of adipocyte growth are largely complementary with Eq. S2, the dynamics of FFAs.

Equation S10 models the positive correlation between an adipocyte's INS$_{on}$ value and its mass. It is well known that an adipocyte's insulin sensitivity negatively correlates with its mass (Salans et al., 1968; Engfeldt and Arner, 1987; Guilherme et al., 2008; Yang et al., 2012). Therefore, $(\text{INS}_{on})_i$, corresponding to the degree of insulin resistance, ought to positively correlate with m_i.

Leanocentric energy balance

The leanocentric energy balance is represented by $\text{E}_{\text{intoLean}}$ = TEE, where TEE is the body's total energy expenditure per day, and $\text{E}_{\text{intoLean}}$ is equal to the energy that enters the lean tissues during the day. $\text{E}_{\text{intoLean}}$ is computed by Eq. S12, namely,

$$\frac{E_{intoLean}}{3} = \int_0^T \Big(\rho_{GLU}\cdot V_{GLU0}\cdot \text{GLU}\cdot\Omega + \rho_{GLU}\cdot U_{myo}\cdot \text{GLU}\cdot\Omega + \rho_{FFA}\cdot u_{FFA0}\cdot N_{myo}\cdot \text{FFA}\cdot\Omega$$
$$+\,\rho_{FFA}\cdot U_{myo}\cdot \text{FFA}\cdot\Omega + \rho_{AA}\cdot u_{AA0}\cdot N_{myo}\cdot \text{AA}\cdot\Omega + \rho_{AA}\cdot U_{myo}\cdot \text{AA}\cdot\Omega\Big)dt.$$

The term $\rho_{GLU}U_{myo}\text{GLU}\Omega$ computes the kilo-calories burned from glucose that enter the muscles during a minute (kcal/min). Indeed, GLU is the plasma glucose concentration, and Ω is the blood volume; thus, ΩGLU is the mass of glucose in the blood. U_{myo} is the rate of muscle glucose uptake (min^{-1}); thus, U_{myo}GLUΩ is the mass of glucose that enters the muscles during a minute (kg/min). The multiplication by ρ_{GLU} converts kilograms of glucose into kilocalories of energy. Similarly, $\rho_{GLU}V_{GLU0}$GLUΩ is the kilocalories generated by basal glucose utilization during a minute; $\rho_{FFA}\,(u_{FFA0}N_{myo}+U_{myo})FFA\Omega$ and $\rho_{AA}\,(u_{AA0}N_{myo}+U_{myo})AA\Omega$ are the kilocalories burned from fat and amino acids, respectively, that enter the muscles during a minute. By summing these values up and then integrating the sum over the entire meal cycle, one obtains

$E_{intoLean}/3$, namely, the total kilocalories that enter the lean tissues during a meal cycle.

Direct application of the ODE model: from $S_{meal}(t)$ to determine TEE

A straightforward application of the ODE model is to start from a given meal supply function $S_{meal}(t)$ to determine $E_{intoLean}$, namely, TEE. The parameters of $S_{meal}(t)$ are all fixed in this paper (see Table S1) except the magnitude A. With a value of A given, the computer simulation is performed for the whole meal cycle (from time 0 to time T) to obtain the time course of all the variables, which are then used by Eq. S12 to calculate $E_{intoLean}$. TEE is also obtained because it is equal to $E_{intoLean}$.

Indirect application of the ODE model: from TEE to determine $S_{meal}(t)$

This paper primarily considers the condition of *necessary feeding*, under which TEE is a prescribed value, and $S_{meal}(t)$ has to be computed to match the given TEE. In other words, the purpose of numerical simulation is to determine the meal magnitude A according to the given TEE. The determination has to be performed by trial and error because the simulation always starts from food intake. Given a trial value of A, the meal function $S_{meal}(t)$ is obtained, and the direct computation (see the last section) is performed to obtain $E_{intoLean}$. If the obtained $E_{intoLean}$ is not sufficiently close to the given TEE, then the simulation is repeated with an updated value of A. After several such trials, the value of $E_{intoLean}$ is sufficiently close to TEE, implying that the correct A, representing the suitable food amount, has been determined.

The clinical data collected from the literature

Table S3 includes the body composition and metabolic data of 44 “subjects” collected from the literature. Each subject actually represents a group of people whose data were averaged in the original literature. The data were used to estimate the three coefficients γ_0, γ_1, and γ_2 in LIFE. Among the 44 total subjects, subjects 1, 2, 3, 4, 17, and 19 had undergone weight perturbation experiments. The post-perturbation data of subjects 1, 2, 3, 4, 17, and 19 are not included in this table but in Table S4.

Table S4 includes the data on subjects 1, 2, 3, 4, 17, and 19 who had undergone weight perturbation experiments. The baseline data were copied from Table S3. The post-perturbation data (marked with asterisks) were taken from the corresponding literature. The data in Table S4 were used to validate the ODE model (see below).

Estimation of the coefficients of the LM-IR-FM Equation (LIFE)

The three coefficients (γ_0, γ_1, γ_2) in LIFE were estimated from the data in Table S3. The scheme of coefficient estimation is as follows. For every subject, an algebraic equation of γ_0, γ_1, and γ_2 only is obtained by substituting the subject's (LM, FM, IR) value into Eq. 6, i.e.,

$$\mathrm{IR} = \gamma_0 \ + \ \gamma_1 \frac{\mathrm{lg(FM)}}{\mathrm{LM} - \gamma_2}.$$

In this way, a set of 44 algebraic equations of γ_0, γ_1, and γ_2 is obtained, from which the values of γ_0, γ_1, and γ_2 can be estimated by a nonlinear fitting program. Unfortunately, what is reported in Table S3 is not (LM, FM, IR) but (LM, FM, TEE). Therefore, for each subject, the IR value must first be obtained by the ODE model. Because the simulation actually starts by using (IR, TEE) to obtain FM, IR must be determined by trial and error. The ODE model is first run with a trial IR and the reported TEE. When the steady state is reached, the simulated FM is obtained. If the simulated FM is sufficiently close to the reported FM, then the trial IR is the desired result. Otherwise, more trials have to be performed until the desired IR is found. After all the subjects' IR values are obtained, the values of γ_0, γ_1, and γ_2 can be estimated. It turns out that only 38 subjects' data are feasible; thus, the three coefficients were actually estimated from 38 algebraic equations.

Following the above scheme, the subjects' IR values were first obtained and are tabulated in Figure 4B. By using the program *NonlinearModelFit* of the software Mathematica (Wolfram Research Inc.), the estimated values $\gamma_0 = 0.664$, $\gamma_1 = 45.4$, and $\gamma_2 = 0$ were obtained. A scatter plot (Figure 4A) was then generated where the 44 dots represent the 44 subjects, whose lg(FM)/LM values are presented along the x-axis and IR values along the y-axis. Among the 44 subjects, there are 38 subjects who demonstrate a linear relationship between IR and lg(FM)/LM; the remaining six subjects (shown within an oval circle) are outliers. The outliers were excluded from the coefficient estimation.

The common feature of the six outliers was their high energy turnover. Their TEE values were the highest among the 44 total, ranging from 3468 (subject 32) to 4493 (subject 41) kcal/day. The

six outliers were all athletes except subject 32, representing the men in the Minnesota Starvation Experiment during the control period (Keys $\mathrm{et\ al.}$, 1950). Although the Minnesota men were not professional athletes, they had an athlete body type because they were specifically selected to survive the upcoming starvation. Furthermore, during the control period they were required to engage in vigorous physical activity, leading to a high rate of energy turnover (TEE = 3468) and high physical activity level (PAL = 2.2) comparable to those of athletes. Therefore, the emergence of outliers was probably because our model parameter values were not applicable to the athletes' special metabolism and physiology. Indeed, for all the simulations the model parameters were fixed to the canonical values (Table S1), which had been estimated from data on sedentary people whose energy turnover ought to be much lower. This explains why the model worked well on the 38 regular subjects, whose TEE values ranged from 1905 to 3155, which were far less than those of the six outliers.

Validation of the ODE model

Table S3 presents the 44 subjects in their baseline (natural, unperturbed) state. Subjects 1, 2, 3, 4, 17, and 19 were perturbed by overfeeding or underfeeding. These subjects are duplicated in Table S4, in both the baseline state (without asterisk) and the post-perturbation, unnatural state (with asterisk). The post-perturbation data were not used to estimate the IR values (Figure 4B). Therefore, they can be used to test the prediction power of the ODE computational model.

As an example, Figure S10A illustrates subject 1, who had IR = 1.5486 and maintained a natural state with FM = 12.0 and TEE = 2481. After several weeks of overfeeding, the subject (now denoted as subject 1*) maintained an unnatural state with FM = 17.1 and TEE = 3110. The question is as follows: can the ODE model accurately predict the unnatural fat mass? We answered the question in the affirmative. By running the model with IR = 1.5486 and TEE = 3110, a steady state was reached at FM = 16.3 kg, which was only 4.6% smaller than the reported FM = 17.1 kg (Figure S10B, the first bar), indicating the accuracy of the prediction. The other subjects were similarly analyzed. The predictions on subjects 1*, 2*, 17*, 17**, 19*, and 19** were all accurate; the predictions on subjects 3* and 4* were reasonably good (Figure S10B). The predicted FM and the reported FM are presented in Figure S10C as the y-coordinate and x-coordinate of the subjects, respectively. Except for subjects 3* and 4*, the dots all accumulate along the diagonal, demonstrating the accuracy of the predictions. It might be more reasonable to compare the predicted lg(FM) with the reported lg(FM) (Figure S10D), which shows that the predictions on subjects 3* and 4* were actually very good, although not as accurate as those on the other subjects. These data suggest the accuracy of the predictions and thus validate the ODE model.

Derivation of Equation 12

Equation 12 is derived from Ohm's law, namely,

$$V = I \times R,$$

$$Q = e^V.$$

The derivation is as follows. First, we have

$$\frac{dQ}{d\mathsf{EI}} = \frac{de^V}{d\mathsf{TEE}} = e^V \frac{dV}{d\mathsf{TEE}} = Q\frac{d\left(I \times R\right)}{d\mathsf{TEE}} = QR\frac{dI}{d\mathsf{TEE}}.$$

Using Eq. g in Figure 6C, namely,

$$I = \frac{\ln 10}{\gamma_1\sigma_1\mathsf{PAL}}\mathsf{TEE} - \frac{\ln 10\sigma_2}{\gamma_1\sigma_1},$$

we have

$$\frac{dQ}{d\mathsf{EI}} = QR\frac{\ln 10}{\gamma_1\sigma_1\mathsf{PAL}}. \tag{S17}$$

Using Eq. 6, namely,

$$\mathsf{IR} = \gamma_0 \ + \ \gamma_1\frac{\mathsf{lg(FM)}}{\mathsf{LM}},$$

we have

$$R = \mathsf{IR} - \gamma_0 = \gamma_1\frac{\lg Q}{\mathsf{LM}}. \tag{S18}$$

Combining Eqs. S17 and S18, we have

$$\begin{aligned}\frac{dQ}{d\mathsf{EI}} &= Q\frac{\gamma_1\lg Q}{\mathsf{LM}}\frac{\ln 10}{\gamma_1\sigma_1\mathsf{PAL}} \\ &= \frac{Q\ln Q}{\sigma_1\mathsf{PAL}\times\mathsf{LM}}.\end{aligned}$$

Because Q actually represents FM, we have

$$d\mathsf{FM} = \frac{\mathsf{FM} \times \ln \mathsf{FM} \times d\mathsf{EI}}{\sigma_1 \times \mathsf{PAL} \times \mathsf{LM}},$$

which is exactly Eq. 12.

References

Abdelmagid, S. A., Clarke, S. E., Nielsen, D. E., Badawi, A., El-Sohemy, A., Mutch, D. M. and Ma, D. W. (2015). Comprehensive profiling of plasma fatty acid concentrations in young healthy Canadian adults. PloS ONE 10, e0116195.

Basu, R., Basu, A., Johnson, C. M., Schwenk, W. F. and Rizza, R. A. (2004). Insulin dose-response curves for stimulation of splanchnic glucose uptake and suppression of endogenous glucose production differ in nondiabetic humans and are abnormal in people with type 2 diabetes. Diabetes 53, 2042–2050.

Bedinger, D. H., Goldfine, I. D., Corbin, J. A., Roell, M. K. and Adams, S. H. (2015). Differential pathway coupling of the activated insulin receptor drives signaling selectivity by XMetA, an allosteric partial agonist antibody. J. Pharmacol. Exp. Ther. 353, 35–43.

Bilous, R. and Donnelly, R. (2010). Handbook of diabetes. John Wiley & Sons.

Bonadonna, R. C., Leif, G., Kraemer, N., Ferrannini, E., Del Prato, S. and DeFronzo, R. A. (1990). Obesity and insulin resistance in humans: a dose-response study. Metabolism 39, 452–459.

Bonadonna, R. C., Saccomani, M. P., Cobelli, C. and DeFronzo, R. A. (1993). Effect of insulin on system A amino acid transport in human skeletal muscle. J. Clin. Invest. 91, 514–521.

Christiansen, E., Garby, L. and Sørensen, T. I. (2005). Quantitative analysis of the energy requirements for development of obesity. J. Theor. Biol. 234, 99–106.

Christiansen, E., Swann, A. and Sørensen, T. I. (2008). Feedback models allowing estimation of thresholds for self-promoting body weight gain. J. Theor. Biol. 254, 731–736.

Cieniewicz, A. M., Kirchner, T., Hinke, S. A., Nanjunda, R., DAquino, K., Boayke, K., Cooper, P. R., Perkinson, R., Chiu, M. L., Jarantow, S. et al. (2017). Novel monoclonal antibody is an allosteric insulin receptor antagonist that induces insulin resistance. Diabetes 66, 206–217.

Cohen, S. L., Halaas, J. L., Friedman, J. M., Chait, B. T., Bennett, L., Chang, D., Hecht, R. and Collins, F. (1996). Human leptin characterization. Nature 382, 589.

Creasy, S. A., Rynders, C. A., Bergouignan, A., Kealey, E. H. and Bessesen, D. H. (2018). Free-Living Responses in Energy Balance to Short-Term Overfeeding in Adults Differing in Propensity for Obesity. Obesity 26, 696–702.

Das, S. K., Roberts, S. B., Bhapkar, M. V., Villareal, D. T., Fontana, L., Martin, C. K., Racette, S. B., Fuss, P. J., Kraus, W. E., Wong, W. W. et al. (2017). Bodycomposition changes in the

Comprehensive Assessment of Long-term Effects of Reducing Intake of Energy (CALERIE)-2 study: a 2-y randomized controlled trial of calorie restriction in nonobese humans. Am. J. Clin. Nutr. 105, 913–927.

Deurenberg, P., Yap, M. and Van Staveren, W. A. (1998). Body mass index and percent body fat: a meta analysis among different ethnic groups. Int. J. Obes. 22, 1164.

Drenowatz, C., Hill, J., Peters, J., Soriano-Maldonado, A. and Blair, S. (2017). The association of change in physical activity and body weight in the regulation of total energy expenditure. Eur. J. Clin. Nutr. 71, 377.

Engfeldt, P. and Arner, P. (1987). Lipolysis in human adipocytes, effects of cell size, age and of regional differences. Horm. Metab. Res. Suppl. 19, 26–29.

Frederich, R. C., Hamann, A., Anderson, S., Löllmann, B., Lowell, B. B. and Flier, J. S. (1995). Leptin levels reflect body lipid content in mice: evidence for diet-induced resistance to leptin action. Nat. Med. 1, 1311–1314.

Geissler, C. A., Miller, D. S. and Shah, M. (1987). The daily metabolic rate of the post-obese and the lean. Am. J. Clin. Nutr. 45, 914–920.

Grund, A., Krause, H., Kraus, M., Siewers, M., Rieckert, H. and Müller, M. (2001). Association between different attributes of physical activity and fat mass in untrained, endurance-and resistance-trained men. Eur. J. App. Phys. 84, 310–320.

Guilherme, A., Virbasius, J. V., Puri, V. and Czech, M. P. (2008). Adipocyte dysfunctions linking obesity to insulin resistance and type 2 diabetes. Nat. Rev. Mol. Cell. Biol. 9, 367–377.

Halaas, J. L., Boozer, C., Blair-West, J., Fidahusein, N., Denton, D. A. and Friedman, J. M. (1997). Physiological response to long-term peripheral and central leptin infusion in lean and obese mice. Proc. Nat. Acad. Sci. USA. 94, 8878–8883.

Hall, K. D. (2006). Computational model of in vivo human energy metabolism during semistarvation and refeeding. Am. J. Physiol. Endocrinol. Metab. 291, E23–E37.

Harris, R. B., Hausman, D. B. and Bartness, T. J. (2002). Compensation for partial lipectomy in mice with genetic alterations of leptin and its receptor subtypes. Am. J. Physiol. Regul. Integr. Comp. Physiol. 283, R1094–R1103.

Havel, R. J., Naimark, A. and Borchgrevink, C. F. (1963). Turnover rate and oxidation of free fatty acids of blood plasma in man during exercise: studies during continuous infusion of palmitate-1-C14. J. Clin. Invest. 42, 1054.

Herman, C. P. and Polivy, J. (1983). A boundary model for the regulation of eating. Psychiat.

Ann. 13, 918–927.

Hintze, L. J., Messier, V., Lavoie, M.-È., Brochu, M., Lavoie, J.-M., Prud'homme, D., Rabasa-Lhoret, R. and Doucet, É. (2018). A one-year resistance training program following weight loss has no significant impact on body composition and energy expenditure in postmenopausal women living with overweight and obesity. Physiol. Behav. 189, 99–106.

Hopkins, M., Finlayson, G., Duarte, C., Gibbons, C., Johnstone, A. M., Whybrow, S., Horgan, G.W., Blundell, J. E. and Stubbs, R. J. (2019). Biological and psychological mediators of the relationships between fat mass, fat-free mass and energy intake. Int. J. Obes. 43, 233.

Horgan, G. W. (2011). The behaviour of a neutral model of weight regulated only by body mass. J. Theor. Biol. 270, 1–6.

Keys, A., Brožek, J., Henschel, A., Mickelsen, O. and Taylor, H. L. (1950). The Biology of Human Starvation. University of Minnesota Press, Minneapolis.

Könner, A. C. and Brüning, J. C. (2012). Selective insulin and leptin resistance in metabolic disorders. Cell Metab. 16, 144–152.

Lee, L. (1998). Volume of blood in a human. The Physics Factbook .

Leibel, R. (2008). Molecular physiology of weight regulation in mice and humans. Int. J. Obes. 32, S98–S108.

Leibel, R. L., Rosenbaum, M. and Hirsch, J. (1995). Changes in energy expenditure resulting from altered body weight. New Engl. J. Med. 332, 621–628.

Levitsky, D. A. (2002). Putting behavior back into feeding behavior: a tribute to George Collier. Appetite 38, 143–148.

Levitsky, D. A. (2005). The non-regulation of food intake in humans: hope for reversing the epidemic of obesity. Phys. Behav. 86, 623–632.

Li, T. and Wang, G. (2014). Computer-aided targeting of the PI3K/Akt/mTOR pathway: Toxicity reduction and therapeutic opportunities. Int. J. Mol. Sci. 15, 18856–18891.

Moro, T., Tinsley, G., Bianco, A., Marcolin, G., Pacelli, Q. F., Battaglia, G., Palma, A., Gentil, P., Neri, M. and Paoli, A. (2016). Effects of eight weeks of time-restricted feeding (16/8) on basal metabolism, maximal strength, body composition, inflammation, and cardiovascular risk factors in resistance-trained males. J. Trans. Med. 14, 290.

Myers, A., Gibbons, C., Finlayson, G. and Blundell, J. (2017). Associations among sedentary and active behaviours, body fat and appetite dysregulation: investigating the myth of physical

inactivity and obesity. Br. J. Sports Med. 51, 1540–1544.

Myers, M. G., Heymsfield, S. B., Haft, C., Kahn, B. B., Laughlin, M., Leibel, R. L., Tschöp, M. H. and Yanovski, J. A. (2012). Challenges and opportunities of defining clinical leptin resistance. Cell Metab. 15, 150–156.

Olefsky, J. M. and Kolterman, O. G. (1981). Mechanisms of insulin resistance in obesity and noninsulin-dependent (type II) diabetes. Am. J. Med. 70, 151–168.

Payne, P. and Dugdale, A. (1977). Mechanisms for the control of body-weight. Lancet 309, 583–586.

Pénicaud, L. (2010). The neural feedback loop between the brain and adipose tissues. In Adipose Tissue Development vol. 19, pp. 84–92. Karger Publishers.

Polonsky, K., Given, B., Hirsch, L., Shapiro, E., Tillil, H., Beebe, C., Galloway, J., Frank, B., Karrison, T. and Van Cauter, E. (1988a). Quantitative study of insulin secretion and clearance in normal and obese subjects. J. Clin. Invest. 81, 435–441.

Polonsky, K., Given, B. and Van Cauter, E. (1988b). Twenty-four hour profiles and pulsatile patterns of insulin secretion in normal and obese subjects. J. Clin. Invest. 81, 442.

Redman, L. M., Kraus, W. E., Bhapkar, M., Das, S. K., Racette, S. B., Martin, C. K., Fontana, L., Wong, W. W., Roberts, S. B. and Ravussin, E. (2013). Energy requirements in nonobese men and women: results from CALERIE. Am. J. Clin. Nutr. 99, 71–78.

Rooks, C., Bennet, T., Bartness, T. J. and Harris, R. B. (2004). Compensation for an increase in body fat caused by donor transplants into mice. Am. J. Physiol. Regul. Integr. Comp. Physiol. 286, R1149–R1155.

Sagayama, H., Yoshimura, E., Yamada, Y., Ichikawa, M., Ebine, N., Higaki, Y., Kiyonaga, A. and Tanaka, H. (2013). Effects of rapid weight loss and regain on body composition and energy expenditure. Appl. Physiol. Nutr. Metab. 39, 21–27.

Salans, L. B., Knittle, J. L. and Hirsch, J. (1968). The role of adipose cell size and adipose tissue insulin sensitivity in the carbohydrate intolerance of human obesity. J. Clin. Invest. 47, 153.

Schulz, L., Nyomba, B., Alger, S., Anderson, T. and Ravussin, E. (1991). Effect of endurance training on sedentary energy expenditure measured in a respiratory chamber. Am. J. Physiol. Endocrinol. Metab. 260, E257–E261.

Shook, R. P., Hand, G. A., Drenowatz, C., Hebert, J. R., Paluch, A. E., Blundell, J. E., Hill, J. O., Katzmarzyk, P. T., Church, T. S. and Blair, S. N. (2015). Low levels of physical activity are

associated with dysregulation of energy intake and fat mass gain over 1 year. Am. J. Clin. Nutr. 102, 1332–1338.

Shook, R. P., Hand, G. A., O'Connor, D. P., Thomas, D. M., Hurley, T. G., Hébert, J. R., Drenowatz, C., Welk, G. J., Carriquiry, A. L. and Blair, S. N. (2018). Energy intake derived from an energy balance equation, validated activity monitors, and dual X-ray absorptiometry can provide acceptable caloric intake data among young adults. J. Nutr. 148, 490–496.

Silva, A. M., Matias, C. N., Santos, D. A., Thomas, D., Bosy-Westphal, A., Müller, M. J., Heymsfield, S. B. and Sardinha, L. B. (2017a). Compensatory Changes in Energy Balance Regulation over One Athletic Season. Med. Sci. Sports Exerc. 49, 1229–1235.

Silva, A. M., Matias, C. N., Santos, D. A., Thomas, D., Bosy-Westphal, A., Müller, M. J., Heymsfield, S. B. and Sardinha, L. B. (2017b). Energy balance over one athletic season. Med. Sci. Sports Exerc. 49, 1724–1733.

Sims, E. A. and Horton, E. S. (1968). Endocrine and metabolic adaptation to obesity and starvation. Am. J. Clin. Nutr. 21, 1455–1470.

Speakman, J. R. (2007). A nonadaptive scenario explaining the genetic predisposition to obesity: the predation release hypothesis. Cell Metab. 6, 5–12.

Speakman, J. R. (2018a). The evolution of body fatness: trading off disease and predation risk. J. Exp. Biol. 221, jeb167254.

Speakman, J. R. (2018b). Why lipostatic set point systems are unlikely to evolve. Mol Metab. 7, 147–154.

Speakman, J. R., Stubbs, R. J. and Mercer, J. G. (2002). Does body mass play a role in the regulation of food intake? Proc. Nutr. Soc. 61, 473–487.

Stumvoll, M., Jacob, S., Wahl, H. G., Hauer, B., Loblein, K., Grauer, P., Becker, R., Nielsen, M., Renn, W. and Haring, H. (2000). Suppression of systemic, intramuscular, and subcutaneous adipose tissue lipolysis by insulin in humans. J. Clin. Endocrinol. Metab. 85, 3740–3745.

Sturis, J., Polonsky, K. S., Mosekilde, E. and Van Cauter, E. (1991). Computer model for mechanisms underlying ultradian oscillations of insulin and glucose. Am. J. Physiol. Endocrinol. Metab. 260, E801–E809.

Svenson, K. L., Von Smith, R., Magnani, P. A., Suetin, H. R., Paigen, B., Naggert, J. K., Li, R., Churchill, G. A. and Peters, L. L. (2007). Multiple trait measurements in 43 inbred mouse strains captures the phenotypic diversity characteristic of human populations. J. App. Phys. 102, 2369–2378.

Tam, J., Fukumura, D. and Jain, R. K. (2009). A mathematical model of murine metabolic regulation by leptin: energy balance and defense of a stable body weight. Cell Metab. 9, 52–63.

Wang, G. (2010). Singularity analysis of the AKT signaling pathway reveals connections between cancer and metabolic diseases. Phys. Biol. 7, 046015–046015.

Wang, G. (2012). Optimal homeostasis necessitates bistable control. J. R. Soc. Interface 9, 2723–2734.

Wang, G. (2014). Raison d'être of insulin resistance: the adjustable threshold hypothesis. J. R. Soc. Interface 11, 20140892.

Weinsier, R. L., Hunter, G. R., Desmond, R. A., Byrne, N. M., Zuckerman, P. A. and Darnell, B. E. (2002). Free-living activity energy expenditure in women successful and unsuccessful at maintaining a normal body weight. Am. J. Clin. Nutr. 75, 499–504.

Weinsier, R. L., Hunter, G. R., Zuckerman, P. A., Redden, D. T., Darnell, B. E., Larson, D. E., Newcomer, B. R. and Goran, M. I. (2000). Energy expenditure and freeliving physical activity in black and white women: comparison before and after weight loss. Am. J. Clin. Nutr. 71, 1138–1146.

Wirtshafter, D. and Davis, J. D. (1977). Set points, settling points, and the control of body weight. Phys. Behav. 19, 75–78.

Yang, J., Eliasson, B., Smith, U., Cushman, S. W. and Sherman, A. S. (2012). The size of large adipose cells is a predictor of insulin resistance in first-degree relatives of type 2 diabetic patients. Obesity 20, 932–938.

Zeng, W., Lu, Y.-H., Lee, J. and Friedman, J. M. (2015). Reanalysis of parabiosis of obesity mutants in the age of leptin. Proc. Nat. Acad. Sci. USA 112, E3874–E3882.